

Quantum criticality around metal-insulator transitions of strongly correlated electrons

Takahiro Misawa and Masatoshi Imada
 Department of Applied Physics, University of Tokyo,
 7-3-1 Hongo, Bunkyo-ku, Tokyo, 113-8656, Japan
 (dated: March 23, 2024)

Quantum criticality of metal-insulator transitions in correlated electron systems is shown to belong to an unconventional universality class with violation of Ginzburg-Landau-Wilson (GLW) scheme formulated for symmetry breaking transitions. This unconventionality arises from an emergent character of the quantum critical point, which appears at the marginal point between the Ising-type symmetry breaking at nonzero temperatures and the topological transition of the Fermi surface at zero temperature. We show that Hartree-Fock approximations of an extended Hubbard model on square lattices are capable of such metal-insulator transitions with unusual criticality under a preexisting symmetry breaking. The obtained universality is consistent with the scaling theory formulated for Mott transition and with a number of numerical results beyond the mean-field level, implying that the preexisting symmetry breaking is not necessarily required for the emergence of this unconventional universality. Examinations of fluctuation effects indicate that the obtained critical exponents remain essentially exact beyond the mean-field level. It further clarifies the whole structure of singularities by a unified treatment of the band-width-control and filling-control transitions. Detailed analyses on the criticality, containing diverging carrier density fluctuations around the marginal quantum critical point, are presented from microscopic calculations and reveal the nature as quantum critical "opalescence". The mechanism of emerging marginal quantum critical point is ascribed to a positive feedback and interplay between the preexisting gap formation present even in metals and kinetic energy gain (loss) of the metallic carrier. Analyses on crossovers between GLW type at nonzero temperature and topological type at zero temperature show that the critical exponents observed in $(V, Cr)_2O_3$ and θ -ET-type organic conductor provide us with evidences for the existence of the present marginal quantum criticality.

PACS numbers: 71.10.Fd, 71.30.+h

I. INTRODUCTION

Metal-insulator (MI) transitions in correlated electron systems have been a challenging subject of studies for decades [1]. In this paper, we show from microscopic analyses that MI transitions of correlated electrons bear an unconventional feature in view of quantum phase transitions. This is shown by taking an example of the Hartree-Fock approximation of the Hubbard model in two dimensions. One might suspect whether the Hartree-Fock approximations could yield a phase transition which is beyond the conventional scheme. However, we show that the simple mean-field approximation allows us to get insight into this issue by capturing the correct interplay of symmetry-breaking and topological characters of the transition. We also discuss that the unconventionality survives beyond the limitation of the mean-field study, where the scaling theory [2, 3] formulated for the Mott transition is applicable. To make the motivation of the present study clearer, we describe somewhat detailed introduction to clarify why the present study has a significance and how the unconventionality arises in view of quantum phase transitions in general. Then in the latter part of the introduction, we review the previous studies on MI transitions to position the starting point.

A. General perspective in view of quantum phase transitions

A ubiquitous example of phase transitions seen in nature is the transition between gas and liquid. At the critical point of the gas-liquid phase transition, the compressibility

$$= \frac{1}{V} \frac{dV}{dP} = \frac{1}{n} \frac{dn}{dP} = \frac{1}{n^2} \frac{dn}{d\mu} \quad (1)$$

and the equivalent density fluctuations $\delta n(r) \delta n(0)$ diverge, where V and μ are the volume and chemical potential, respectively. The opalescence observed in light scattering is caused by such diverging density fluctuations. Nearly a century ago, the critical opalescence found in the scale of the light wave length was analyzed by Ornstein, Zernike [4], Einstein and Smoluchovski [5, 6] as one of the evidences for the existence of atoms.

The gas-liquid transition is mapped to the ferromagnetic transition in the Ising model with the Z_2 symmetry expressed by the Hamiltonian

$$H = \sum_{\langle i,j \rangle} J_{ij} S_i S_j - h \sum_i S_i; \quad (2)$$

for the local spin S_i taking ± 1 at the site i , and interacting with short-ranged neighbors at j and under the symmetry breaking field h . The Ising model represents the simplest example that phase transitions in general

Electronic address: misawa@solist.u-tokyo.ac.jp

take place because of a spontaneous breaking of symmetries originally hold in the Hamiltonian at $h = 0$. Although the gas-liquid transition at a first glance does not look breaking the symmetry as in the ordered phase of the Ising model, the transition is actually mapped to the Z_2 symmetry breaking along the first-order coexistence boundary. In fact, the up and down spin phases in the Ising model are mapped to the gas and liquid phases, respectively, from which the both transitions turn out to belong to the same universality class. In more general, thermal phase transitions are all characterized by a certain type of spontaneous symmetry breakings.

Phase transitions by the conventional spontaneous symmetry breaking is correctly described by the Ginzburg-Landau-Wilson (GLW) scheme [7, 8, 9]. In this scheme, the free energy F is expressed by a functional of a spatially dependent order parameter $m(\mathbf{r})$ after eliminating other degrees of freedom. F is assumed to allow a regular expansion with respect to $m(\mathbf{r})$ such as

$$F = \int d\mathbf{r} \left[\frac{1}{2} (\nabla m(\mathbf{r}))^2 + \frac{a}{2!} m(\mathbf{r})^2 + \frac{K}{2!} (\nabla m(\mathbf{r}))^2 + \frac{b}{4!} m(\mathbf{r})^4 + \dots \right];$$

where b and K are positive constants and the coefficient a depends on the control parameter g around the critical point g_c as $a = a_0(g - g_c)$.

This classical picture of the phase transitions is modified in quantum systems. For instance, when the transverse field ΓS_i^x is additionally applied to the Ising model (2) by considering spin-1/2 quantum spins $S_i = (S_i^x; S_i^y; S_i^z)$, T_c is suppressed to zero at a critical value g_c and the transition disappears as illustrated in Fig. 1. This may be regarded as a destruction of the symmetry broken order by quantum fluctuations instead of thermal fluctuations.

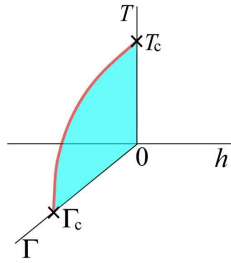


FIG. 1: (color online) Schematic phase diagram of Ising model under longitudinal and transverse magnetic fields, h and Γ , respectively. Up and down spin phases are separated by the first-order boundary illustrated by shaded (blue) sheet below the critical line shown by bold (brown) curve in parameter space of T , h and the transverse Ising field Γ . Beyond the quantum critical point at g_c , the transition disappears and the up and down spin phases are adiabatically connected even through the route on the $T = 0$ plane.

In fact, a quantum system may be expressed in the path integral formalism, where an additional dimension

representing the imaginary time or inverse-temperature axis is introduced in addition to the d -dimensional spatial degrees of freedom. Although the added imaginary time direction could be qualitatively different from the spatial dimensions, one can show that it simply corresponds to z additional spatial dimensions, where z is called the dynamical exponent. The transverse Ising model is simply represented by $z = 1$. Namely, the quantum phase transition at $T = 0$ in d spatial dimensions realized by increasing Γ to Γ_c may be mapped to the transition at nonzero temperature in $d + 1$ dimensional classical systems [10].

However, in more general, if the quantum dynamics has a coupling to dissipative gapless excitations such as particle-hole excitations in metals, z may become larger than unity such as two or three [11, 12, 13]. Ferromagnetic and antiferromagnetic phase transitions in metals have been extensively studied from this viewpoint. The quantum critical point appears when the critical temperature is lowered to zero. Around the quantum critical point, low-energy excitations arising from growing magnetic correlations have been proposed to cause non-Fermi liquid properties [11, 12, 13]. A particular type of metamagnetic transitions has also been studied around the "quantum critical end point" [14], where an apparent symmetry does not change at the critical point, whereas an implicit symmetry breaking does occur as in the case of the gas-liquid transition. Even in these cases with z larger than unity, however, the GLW scheme remains essentially valid when we consider a proper $d + z$ -dimensional system.

Here the dynamical exponent z is defined from the ratio of the temporal correlation length τ to the spatial one ξ of the order parameter $m(\mathbf{r}; t)$ in d dimensions. In the case of conventional quantum phase transitions, τ and ξ are defined by

$$\xi = \lim_{r \rightarrow \infty} \frac{\log |m(\mathbf{r}; 0) m(\mathbf{0}; 0)|}{r}; \quad (4)$$

$$\tau = \lim_{t \rightarrow \infty} \frac{\log |m(\mathbf{0}; t) m(\mathbf{0}; 0)|}{t}; \quad (5)$$

respectively. More concretely, the dynamical exponent z is defined in the asymptotic limit to the critical point $g \rightarrow g_c$ by

$$z = \lim_{g \rightarrow g_c} \frac{\log \tau}{\log \xi}; \quad (6)$$

As we will show in the next subsection, in the case of the metal-insulator transitions, these definitions should be modified, because the correlations in metals decay not exponentially but with power laws as a function of distance in general.

In contrast to the description of the phase transition by the symmetry breaking, several classes of quantum phase transitions at $T = 0$ are not captured by such extensions of the GLW scheme and are not characterized by the spontaneous symmetry breaking. One of the simplest

examples is found in the transition between a metal and a band insulator. The ground-state energy E of noninteracting electrons near the parabolic band bottom with the single-particle dispersion $\epsilon = AK^2$ in d dimensions is obviously described by

$$E/n^{(d+2)/d} \propto n^{(d+2)/2}; \quad (7)$$

in the metallic phase for the electron density n and the chemical potential measured from the band bottom. On the other hand, throughout the insulating phase with the chemical potential varied in the gap, $E = 0$ holds because of $n = 0$. This trivially nonanalytic form of the energy as a function of μ clearly represents a quantum phase transition with the singularity at $\mu = 0$, but it is equally obvious that it does not follow the GLW scheme. This transition of noninteracting fermions is not accompanied by any kind of spontaneous symmetry breaking. It is rather characterized only by the presence or absence of the Fermi surface, which is a topological difference. Wen [15] has proposed a category of "quantum orders" for this class of transitions.

In this paper, we show that an involved interplay of the topological nature at $T = 0$ with the conventional GLW character at $T \neq 0$ emerges for metal-insulator (MI) transitions of correlated electrons. By controlling a parameter for quantum fluctuations, a zero-temperature critical line characterized by the topological transition of Fermi surface from a metal to an insulator switches over to a finite-temperature critical line characterized by GLW scheme. The phase diagram is now seriously modified from Fig. 1 to a new type depicted in Fig. 2. Here, the quantum critical point is turned into the starting point (or end point) of the quantum critical line which represents topological nature of transitions at $T = 0$. We call this starting and marginal quantum critical point (MQCP), which is completely different from the conventional quantum critical point. Then electron correlation effects generate an unconventional universality class of phase transitions, which is expected neither in GLW category nor in simple topological transitions.

B. Introduction for metal-insulator transitions

Now we summarize understanding of MI transitions for strongly correlated electrons achieved in preceding studies in the literature to make clear our motivation of the present study. This issue has attracted long-standing interest and various important aspects have been clarified [1], although complete understanding has not been reached. MI transitions may occur with coupling to lattice distortions or be accompanied by effects of randomness in real materials. However, purely electronic origin of MI transitions has been a central issue in the strong correlation regime, where we find many examples called Mott transition. For this purpose, Hubbard model, which only considers the local Coulomb interaction on a lattice,

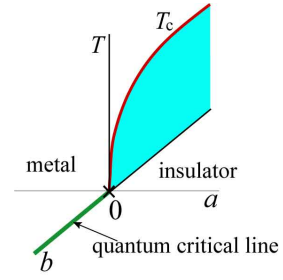


FIG. 2: (color online) Proposed phase diagram of MI transition for strongly correlated electron systems. A crucial difference from Fig. 1 is that the quantum critical line starts along the a -axis (the thick (green) line along $a = T = 0$) beyond the endpoint of the first-order boundary called marginal quantum critical point depicted by the cross. This difference is a direct consequence of the topological nature of MI transition at $T = 0$. Here the first-order boundary is again shown by the shaded (blue) surface.

is one of the simplest models to describe MI transitions. Hubbard model is defined by the Hamiltonian as

$$H = \sum_{i,j} \sum_{\sigma} t_{ij} c_{i\sigma}^{\dagger} c_{j\sigma} + U \sum_i n_{i\uparrow} n_{i\downarrow} - \sum_i \mu n_i; \quad (8)$$

where c_i^{\dagger} (c_i) creates (annihilates) an electron with spin at site i , respectively. The number operator is n_i and μ represents the chemical potential. Hopping integral between site i and j is represented by t_{ij} and U denotes the onsite Coulomb repulsion.

Approximate and simple theoretical descriptions of the Mott transition at $T = 0$ without any symmetry breaking being involved was proposed in seminal works of Hubbard [16] and Brinkman and Rice [17]. These two works offer completely different pictures for the transition. Hubbard approximation offers a picture of simple splitting of a band into an upper and a lower band with a gap between these two bands. The transition to Mott insulator occurs simply because the chemical potential moves into the gap. The "quasiparticle" weight Z at the Fermi level is retained nonzero even at the transition, although the "large Fermi surface" with the Luttinger volume is not preserved and a small pocket of the Fermi surface shrinks to zero at the transition. Brinkman-Rice picture obtained from the Gutzwiller approximation, in contrast, preserves the Luttinger volume and the Mott insulator is realized by the vanishing quasiparticle weight Z . Dynamical mean-field theory (DMFT) [18] proposed some unification of these two pictures with the formation of the upper and lower Hubbard bands reproduced together with the vanishing Z in the coherent additional "band". In DMFT results, the Mott transition itself is triggered by the vanishing coherent band and the criticality is ultimately determined from that of the Brinkman-Rice scenario.

Recently, DMFT has been improved by taking into account the momentum dependence of the self-energy in

the correlator projection method [19]. The Mott transition obtained from this improvement shows that a transition qualitatively different from the original DMFT scenario occurs, where the renormalization factor Z is kept nonzero until the transition [20]. Instead of vanishing Z , the transition is realized by shrinkage and vanishing of the Fermi-surface pocket with some similarity to the Hubbard picture. A crucial difference from the Hubbard picture is that the upper and lower Hubbard bands may have qualitatively different dispersions accompanied by electron differentiation in momentum space [9, 21, 22]. The vanishing pocket looks to show very anisotropic spectral weight with strong intensity on the inner-half circle and weak intensity on the outer-half circle, making an apparent arc-type structure for the model on the square lattice. This arc-type structure is consistent with the experimental observations in the copper oxides obtained from angle resolved photoemission spectra (ARPES) [23, 24]. This Fermi-surface pocket appears after the Lifshitz transition within the metallic phase, where the topology of the Fermi surface changes from that of a large Fermi surface to pockets. Such Lifshitz transitions seem to inevitably occur, which invalidates the Luttinger theorem after the transition to the pockets [20]. A similar conclusion was obtained by cellular DMFT study for system with a one-dimensional anisotropy [25] as well as in 2D [27], and by dynamical cluster approximation for 2D Hubbard model [26], where the momentum dependence of the self-energy was considered in different ways. The serious modification of DMFT and the complete change in the nature of the MI transition with vanishing pocket of the Fermi surface seems to have a deep connection to the satisfaction of the hyperscaling and a momentum-space differentiation as we discuss below.

A picture of MI transitions completely different from various mean-field approximations including DMFT has been proposed from the scaling theory of Mott transition [2, 3], where the singularity of the free energy F at the Mott transition is assumed to follow the hyperscaling form

$$F \sim \xi^{-(d+z)}; \quad (9)$$

Here, ξ in the metallic side is the correlation length defined by $\xi^{-1=d}$ for the metallic carrier concentration X and spatial dimensionality d , while it is the localization length of carriers in the insulating side. More precise definition of ξ should be given from the correlation length of the order-parameter correlation function, which will be discussed in the end of this section and will be clarified that the above relation is correct. The hyperscaling is normally satisfied below the upper critical dimension d_u , whereas the mean-field theories are satisfied above d_u . Therefore, the scaling theory and various mean-field theories are incompatible in general.

Before proceeding to more involved discussions on the scaling theory, we briefly summarize basic points of critical phenomena and universality classes particularly for metal-insulator transitions used in the later discussions.

The universality class of phase transitions is characterized by critical exponents. We first discuss relations for critical exponents which is applicable irrespective of the validity of either the hyperscaling or mean-field approximations. When we take the carrier concentration X as the order parameter in the metallic side, the critical exponent is defined by

$$X \sim t^{-1/\nu}; \quad (10)$$

which measures the scaling behavior of the growth of the order parameter as a function of the field t , which is conjugate to the order parameter X . Namely, ν is either the chemical potential for the filling-control transition or $U-t$ in the Hubbard model for the band-width control transition. In the latter case, ν is, for example, controlled by pressure P in actual experiments. The carrier concentration X is the doping concentration itself for the filling-control case while it is the unbound doublon (doubly occupied sites) and holon (empty site) concentrations measured from the values at the critical point for the band-width control case.

The exponent ν is defined from the relation of the control parameter g to ν as

$$g \sim \nu^{-1/\nu}; \quad (11)$$

Here, the control parameter g may also be controlled by $U-t$ or μ , which makes some complexity and could cause a confusion, because these two quantities can control both of ν and g . This is somehow in contrast with the simple case of Eq. (3), where h and a may be controlled independently, say, by the magnetic field and temperature, respectively. In the later microscopic description in Sec. III, this somewhat confusing situation will be resolved.

The exponent ν is defined from the order-parameter susceptibility $\chi = dX/d\mu$ from the scaling

$$\chi \sim \nu^{-1/\nu}; \quad (12)$$

The jump of X at the first-order boundary grows from the critical point as

$$X \sim \nu^{-1/\nu}; \quad (13)$$

The exponent ν is obtained from the second derivative of the free energy as

$$d^2F/dg^2 \sim \nu^{-1/\nu}; \quad (14)$$

It should be noted that for quantum phase transitions does not express the exponent for the specific heat as in thermal transitions. The set of these exponents has a significant meaning because the set specifies the fundamental nature of the phase transitions called the universality class.

Conventional scaling laws such as Widom's law

$$(\chi - 1) = \nu^{-1/\nu}; \quad (15)$$

and Rushbrooke's law

$$\beta + 2 + \gamma = 2 \quad (16)$$

may be satisfied for these exponents. So far, the control parameter g is not fixed yet and one may have several choices. Some of the exponents need trivial transformation depending on the definition of g [8].

When the hyperscaling assumption is employed, the length scale which diverges toward the critical point is unique, and it must be the mean carrier distance given by

$$\ell / X^{1/d}; \quad (17)$$

Then the free energy expressed by Eq. (9) leads to

$$F / X^{(d+z)=d}; \quad (18)$$

This is the form at $\mu = 0$ and $g = g_c = 0$. Scaling relations are derived by further adding the term of the "chemical potential" and the term of coupling to $g = g_c$ as

$$F = -X + B_0(g - g_c)X + C X^{(d+z)=d}; \quad (19)$$

where B_0 and C are constants and μ should be separately given from a physical consideration or microscopic derivation of the transition. Note that the definition of g is now fixed as the quantity to control the transition at $\mu = 0$. The scaling between X and μ , namely, Eq. (10) is obtained by putting $g = g_c = 0$ in Eq. (19) and minimize the free energy by $dF/dX = 0$. This yields

$$\mu = z/d; \quad (20)$$

The scalings between X and g , namely, Eqs. (12) and (13) are obtained by putting $\mu = 0$ in Eq. (19) and minimize the free energy by $dF/dg = 0$. This yields

$$\frac{dX}{dg} = \frac{1}{1 + z/d}; \quad (21)$$

and

$$\frac{d^2X}{dg^2} = \frac{z/d}{z + d(1 + z/d)}; \quad (22)$$

From (11), (13) and (17), a further relation

$$\frac{d^2X}{dg^2} = -d \quad (23)$$

is obtained. Note that the scaling laws Eqs. (15) and (16) are obviously satisfied for Eqs. (20)–(23). From the scalings (9), (11) and (17), we obtain $F / \mu^{(d+z)}$ for nonzero $g = g_c$. From this and Eq. (14), the Josephson relation

$$\frac{D}{X} = 2(d + z) \quad (24)$$

is obtained. In addition, Druide weight is shown to follow [1]

$$D / X^{1+(z-2)=d}; \quad (25)$$

To estimate accurate exponents of microscopic models, in principle, one needs to go beyond the mean-field approximation, because the reliability of the mean-field approximation itself has to be critically tested. Available theoretical tools for this purpose is severely limited, because of various difficulties in theoretical approaches for strongly correlated electrons. In the literature, there exist only small number of available estimates from unbiased approaches such as the quantum Monte Carlo and path-integral renormalization group methods. For the filling-control transition of Hubbard model or the t - J model on a square lattice, by using the quantum Monte Carlo method [29, 30, 31] and power Lanczos method [32], the charge compressibility has been shown to follow the scaling $dX/d\mu \propto X^{-1}$, from which β is estimated from Eq. (10) as $\beta = 2$. The result obtained from the path-integral renormalization group method is also consistent with this scaling [35]. When the hyperscaling holds, $\beta = 2$ and Eq. (20) in two dimensions leads to $z = 4$. On the other hand, simple GLW scheme always gives $\beta > 3$ and is incompatible with the numerical results. In fact, the exponents of the Ising model are $\beta = 4/8$ for three-dimensional systems and $\beta = 15$ in two dimensions. Any other types of symmetry breakings indicate $\beta > 3$. Note also that the degeneracy temperature (effective Fermi temperature) T_F is scaled by $T_F / \mu^{1/z} \propto X^{z/d}$ resulting in T_F / X^2 for $z = 4$ and $d = 2$, if the hyperscaling is satisfied [3].

Experimentally, the exponent β has been examined for filling-control transitions by measuring the chemical potential shift with increasing doping by photoemission studies in several high- T_c copper oxides [39, 40]. In particular, $\text{Bi}_2\text{Sr}_2\text{CaCu}_2\text{O}_{8+y}$ and $(\text{La,Sr})_2\text{CuO}_4$ show pinnings of the chemical potential at low doping, indicating an enhancement of the charge compressibility and consistency with $\beta = 2$. ^3He adsorbed on a graphite surface, offering a unique two-dimensional fermion system with strong correlation effects, appears to show an anomalous suppression of T_F near the commensurate solid phase in accordance with the trend of T_F / X^2 consistently with $z = 4$ [41] with the hyperscaling being satisfied.

In addition, the Druide weight has been calculated to be consistent with D / X^2 [33, 34] which suggests $z = 4$ from the above relation (25) if the hyperscaling is satisfied. These two independent estimates of z coincide each other and support the hyperscaling.

Other exponents are directly related to g dependence of F and it is fixed when β is specified. If one put $z = 4$ and $d = 2$,

$$\beta = \frac{1}{2(3 - \beta)}; \quad (26)$$

$$\beta = 2 - \frac{1}{3 - \beta}; \quad (27)$$

$$\beta = \frac{1}{3} \quad (28)$$

and

$$= \frac{1}{3} \quad (29)$$

are obtained.

This unconventional universality class has further been analyzed and $\nu = 2$ is obtained from a plausible assumption on the quasiparticle dispersion [36, 37, 38]. Then, the universality class is proposed to be characterized by a set of the exponents

$$z = 4; \nu = 1; \beta = 1; \gamma = 1; \delta = 2; \eta = 1/2 \text{ and } \theta = 0: \quad (30)$$

At finite temperatures, it has been theoretically proposed that the M I transition is equivalent to the gas-liquid transition and its universality class belongs to the Ising universality class [42, 43]. Experimentally, from recent careful study of V_2O_3 by Lin et al [44], they have obtained the critical exponents which are consistent with that of the 3D Ising model, namely, $\beta = 0.34$, $\gamma = 1.0$ and $\nu = 1.0$ in the region very close to the critical point whereas they have obtained consistency with the mean field exponents for the Ising model in the most part away from the critical point. On the contrary, recent experimental results on $-(ET)_2Cu[N(CN)_2]Cl$ [45, 46] indicate the critical exponents $\beta = 1$; $\gamma = 1$ and $\nu = 2$, which are consistent with Eq. (30) and indicates an evidence for the relevance of the present universality.

Before closing this section, we remark on the definition of ν and the dynamical exponent z . In the case of M I transitions, correlation functions do not decay exponentially as a function of distance in the metallic phase. Therefore, the conventional definition of ν given in Eq. (4) is not applied. For example, noninteracting electrons have a density-density correlation function $\chi(r)X(0)i$ which asymptotically decays as $1/r^3$ with Friedel oscillations in two-dimensions [30]. Such an asymptotic decay crosses over to a constant at shorter distance, where the crossover length is determined from the inverse of Fermi wave number k_F . Since $1/r^3$ decay is absolutely convergent in the integration, the integration over distance is contributed dominantly from the region inside of the length scale of k_F^{-1} . From this, ν is given by $\nu = 1/k_F^{-1} / X(0) = d$. More precisely, the correlation length is defined by

$$\nu = \frac{\int_0^\infty dr \chi(r;0)X(0;0)i}{\chi(0;0)X(0;0)i} \quad (31)$$

In the similar way, the temporal correlation length τ is defined by

$$\tau = \frac{\int_0^\infty dt \chi(0;t)X(0;0)i}{\chi(0;0)X(0;0)i} \quad (32)$$

Then the dynamical exponent z is obtained from

$$z = \lim_{g \rightarrow g_c} \frac{\log \nu}{\log g}; \quad (33)$$

where we have used relations for the equal-time structure factor S and susceptibility χ , given by

$$S = \frac{1}{N} \sum_{\mathbf{r}} \chi(\mathbf{r};0)X(0;0)i / \nu^d \quad (34)$$

$$\chi = \frac{1}{N} \sum_{\mathbf{r}} \chi(\mathbf{r};t)X(0;0)i / \nu^{z+d} \quad (35)$$

leading to

$$\frac{\nu}{S} \propto \nu^z; \quad (36)$$

C. Outline of the present work

In this paper, we show that the basic structure of the phase diagram for the M I transition involving the quantum critical line and the boundary for the first-order transition is correctly captured by the Hartree-Fock theory of the Hubbard model. A remarkable result in this paper is that the Hartree-Fock approximation is able to derive the above unconventional universality class at M QCP from a microscopic derivation of the free energy. The obtained universality class turns out to be consistent with the scaling theory. The mechanism of the emergence of M QCP and resultant unconventional universality is clarified from the present microscopic study. It is ascribed to the selfconsistent positive feedback between metallic carrier density and the amplitude of an insulating gap already developed in metals. More concretely, increase of the preformed gap amplitude decreases the carrier density to lower the kinetic energy, which in turn further enhances the preformed gap. On the contrary, the decreasing preformed gap allows more carriers, which further reduce the gap to gain the kinetic energy of carriers. These nonlinear effects cause the first-order transition and M QCP emerges at the border between the first-order transition and the quantum critical line. Furthermore, the Hartree-Fock theory turns out to remain essentially correct even when one goes beyond the mean-field approximation and takes into account quantum fluctuations. This is because the transition always occurs at that at the upper critical dimension irrespective of the spatial dimensionality. We further show that the Hartree-Fock solution has a finite-temperature crossover to the conventional Ising universality class. We discuss implications and consequences of this unexplored type of universality class emerging near M QCP sandwiched by GLW critical and quantum critical lines. We argue that low-energy excitations are described neither by the original single-particle picture nor by the bosonic density fluctuations when the both characters of transitions meet.

We also discuss comparison of the present result with the experimental indications obtained so far. It is shown that the critical exponents at M QCP together with the finite-temperature crossover are completely consistent with the whole aspects of the experimental results.

A part of the discussions in this paper is already briefly given [49]. In this paper, we present the results of quantum M I transitions in greater detail. In particular, we show details of the procedure to obtain the non-GLW free-energy expansion and critical exponents together with thorough discussions on implications.

The organization of this paper is as follows: In Sec. II, we show details of our Hartree-Fock approximation. In Sec. III, we present Hartree-Fock solutions of the M I transition by introducing the preexisting order parameter. It captures some essence of the unconventional universality class of the transition from metals to insulators caused by the electron correlation effects. Using the free-energy expansion, we analytically obtain the critical exponents of quantum M I transitions, which belongs to an unconventional universality. We also discuss implications beyond the mean-field approximations in Sec. III. In Sec. IV, we show numerical results of Hartree-Fock approximation at $T = 0$, which are completely consistent with the analytical results in Sec. III. In Sec. V, finite-temperature crossover is calculated. It shows a well-defined crossover from the Ising universality in the close vicinity of the critical point to the quantum universality governed by MQCP when the parameter deviates from the critical point. Section VI describes comparisons of the present implications with relevant experimental results. Section VII is devoted to summary and discussions.

II. HARTREE-FOCK APPROXIMATION

In this paper, to capture the essence of quantum M I transitions, we extend Hubbard model (8) by considering the nearest-neighbor repulsion term proportional to V on the $N_s = L \times L$ square lattice. It is defined by

$$H = \sum_{\mathbf{k}} (t_1(\mathbf{k}) + t_2(\mathbf{k})) c_{\mathbf{k}}^y c_{\mathbf{k}} + U \sum_i n_{i\uparrow} n_{i\downarrow} + V \sum_{\langle ij \rangle} N_i N_j + \sum_i N_i; \quad (37)$$

where $N_i = (n_{i\uparrow} + n_{i\downarrow})$ are number operators. We restrict the hopping terms to the nearest neighbor pairs given by the dispersion $t_1(\mathbf{k}) = 2t(\cos k_x + \cos k_y)$ and that of the next-nearest neighbor pairs by $t_2(\mathbf{k}) = 4t^0 \cos k_x \cos k_y$, respectively.

Using this extended Hubbard model, we study quantum M I transitions in two-dimensional system within the Hartree-Fock approximation. Although the Hartree-Fock analyses have been done for the Hubbard model in the literature [47, 48], the criticality of M I transitions has not been examined. By considering the M I transitions in the ordered phase, we are able to capture a remarkable aspect of M I transitions from a microscopic model.

To consider the M I transitions within the Hartree-Fock approximation, we consider a symmetry broken long-range order such as charge or antiferromagnetic (AF) ordering with the periodicity commensurate to the lattice.

Then we study the M I transitions in the symmetry broken phase. We note that essence of the M I transitions does not depend on the type of the ordering. For the extended Hubbard model defined in Eq. (8), two simple orders become stable. When $4V > U$, the extended Hubbard model has a tendency to charge ordering, where the empty and doubly occupied sites alternately align within the mean-field level. The order parameter of checker-board-type doublon alignment is defined by

$$m = \frac{1}{N_s} \sum_i h(n_{i\uparrow} + n_{i\downarrow}) \exp(i\mathbf{Q} \cdot \mathbf{r}_i); \quad (38)$$

where \mathbf{Q} is the ordering wave vector (π, π). For $U > 4V$, the antiferromagnetic ordering becomes stable. The order parameter of the antiferromagnetic ordering m_{AF} is defined by

$$m_{AF} = \frac{1}{N_s} \sum_i h(n_{i\uparrow} - n_{i\downarrow}) \exp(i\mathbf{Q} \cdot \mathbf{r}_i); \quad (39)$$

Hereafter, we mainly consider the charge ordering. However, within the mean-field approximation, the antiferromagnetic order and charge order play the same role on M I transition and by replacing the order parameter with the antiferromagnetic one, one can easily reach the same results for the nature of the M I transition.

Here we take the mean-field as

$$h n_{i\uparrow} = h n_{i\downarrow} = \frac{(n + m \exp(i\mathbf{Q} \cdot \mathbf{r}_i))}{2}; \quad (40)$$

with \bar{n} being the average charge density given by $\bar{n} = \frac{1}{N_s} \sum_i h n_{i\uparrow} + h n_{i\downarrow}$. Using this mean-field, we decouple the interaction term.

The on-site interaction term is decoupled as

$$\begin{aligned} U \sum_i n_{i\uparrow} n_{i\downarrow} &= U \sum_i (n_{i\uparrow} h n_{i\downarrow} + n_{i\downarrow} h n_{i\uparrow} - h n_{i\uparrow} h n_{i\downarrow}) \\ &= \frac{U}{2} \sum_i n_i (n + m \exp(i\mathbf{Q} \cdot \mathbf{r}_i)) \\ &= \frac{U N_s (n^2 + m^2)}{4}; \end{aligned} \quad (41)$$

The nearest-neighbor interaction term is decoupled as

$$\begin{aligned} V \sum_{\langle ij \rangle} N_i N_j &= V \sum_{\langle ij \rangle} (N_i h N_j + N_j h N_i - h N_i h N_j) \\ &= 4nV \sum_i N_i + 4mV \sum_i N_i \exp(i\mathbf{Q} \cdot \mathbf{r}_i) \\ &= 2V N_s (n^2 + m^2); \end{aligned} \quad (42)$$

Finally we obtain a Hartree-Fock Hamiltonian (H_{HF}) in the momentum space as

$$\begin{aligned} H_{HF} &= \sum_{\mathbf{k}} (t_1(\mathbf{k}) + t_2(\mathbf{k})) \frac{U n}{2} + 4nV \sum_{\mathbf{k}} c_{\mathbf{k}}^y c_{\mathbf{k}} \\ &+ \frac{U}{2} \sum_{\mathbf{k}} (4V - m \sum_{\mathbf{k}} c_{\mathbf{k}+\mathbf{Q}}^y c_{\mathbf{k}}) \\ &+ \frac{U N_s (n^2 + m^2)}{4} + 2V N_s (n^2 + m^2); \end{aligned} \quad (43)$$

where we define $\epsilon(k) = \epsilon_1(k) + \epsilon_2(k)$.

Diagonalizing the Hamiltonian leads to two bands of the form

$$E_{\pm} = \epsilon_2(k) \pm \sqrt{\epsilon_1(k)^2 + t^2}; \quad (44)$$

where $t = mg$ and we now take $g = 4V \frac{U}{2}$ as the control parameter, because in this section we mainly consider the band-width control transition. In Eq. (44), we dropped a constant term $n(g + U)$.

Using this Hartree-Fock band dispersion we obtain the free energy

$$\begin{aligned} F_{\text{HF}} &= \frac{T}{N_s} \log Z_{\text{HF}} \\ &= \frac{2T}{N_s} \sum_k \log [1 + \exp(-\frac{E_{\pm}(k)}{T})] \\ &\quad - \frac{U(n^2 + m^2)}{4} + 2V(n^2 - m^2); \end{aligned} \quad (45)$$

where the sum takes

From this free energy, the order parameter m is determined from the self-consistency condition

$$\frac{1}{g} = \frac{2}{N_s} \sum_k \frac{f(E_{-}(k)) - f(E_{+}(k))}{E_{+}(k) - E_{-}(k)}; \quad (46)$$

where $f(x)$ is the Fermi-Dirac distribution function. The particle density n is given by

$$n = \frac{1}{N_s} \sum_k [f(E_{-}(k)) + f(E_{+}(k))]; \quad (47)$$

Details of numerical calculations of Eqs. (46) and (47) are shown in Appendix A.

It turns out that the self-consistent equation (46) with Eq. (44) for the charge ordering is equivalent to the self-consistent equation for the AF ordering defined in Eq. (39) [47, 48]. The equivalence holds by replacing the charge order parameter m with the antiferromagnetic (AF) order parameter m_{AF} and by putting $g = U/2$. However, one should be careful about this mapping. This mapping is complete only on the Hartree-Fock level. The charge ordering at the $(\pi; \pi)$ periodicity is the consequence of the discrete symmetry breaking while the AF ordering is realized by the continuous symmetry breaking of $SU(2)$ symmetry. Therefore, if it would be exactly solved in two-dimensional systems, the charge ordering can indeed exist at finite temperatures, though AF ordering cannot exist at finite temperatures by Mermin-Wagner theorem. Therefore, the Hartree-Fock approximation captures some essence of the charge ordering at finite temperatures, while the AF ordering at nonzero temperatures in two dimensions contains an artifact of the Hartree-Fock approximation, although the development of the charge gap itself is not an artifact, which leads to the Mott gap formation even without any long-range order. The physics of unconventional quantum criticality, which we clarify later, emerges from the gap formation itself and therefore the essence is captured in the Hartree-Fock calculation.

III. FREE-ENERGY EXPANSION AND CRITICAL EXPONENTS

In this section, we analyze singularities of the free energy around the MI transition within the Hartree-Fock approximation at $T = 0$ and obtain the critical exponents of the transition. When the order parameter m and the gap $\Delta = mg$ are sufficiently small near the charge-order or antiferromagnetic transition, the insulating gap does not open for nonzero positive t^0 . This is because, the upper band E_{+} and lower band E_{-} overlap for a small gap. From Eq. (44), the top [bottom] of the lower [upper] band is located at $(k_x; k_y) = (\pm 2; \pm 2) [(\pm 2; 0)]$, respectively. The continuous MI transition occurs when the top of the lower band reaches the same energy as that of the bottom of the upper band as shown in Fig. 3. Therefore, the condition of the continuous MI transition is given by

$$E_{+}(\pm 2; 0; c) = E_{-}(\pm 2; \pm 2; c); \quad (48)$$

where c is the critical gap of the continuous MI transition. From this, at $T = 0$, we obtain the critical gap c as

$$c = 2t^0; \quad (49)$$

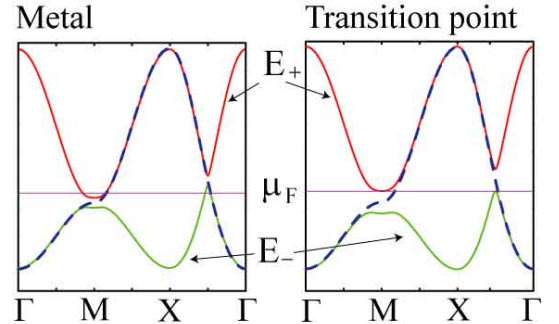


FIG. 3: (color online) Quasiparticle band structures of the Hartree-Fock solution for metallic phase (left) and the continuous MI transition point (right) are shown. Broken (blue) line shows the free-particle band dispersion defined by $\epsilon(k) = 2t(\cos k_x + \cos k_y) + 4t^0 \cos k_x \cos k_y$. The definition of the upper (lower) band is defined in Eq. (44). Fermi energy μ_F is represented by the horizontal line. In the metallic phase, the bottom of the upper band at M point $(\pi; 0)$ and its equivalent points is lower than the top of the lower band at $(\pm 2; \pm 2)$ and its equivalent points so that the indirect insulating gap is closed.

This quantum MI transition occurs between charge-ordered metal and charge-ordered insulator, thus the symmetry does not change at the transition. It is legitimate to expand the free energy around nonzero order parameter m measured from the critical point of the MI transition. One might speculate that the free energy expressed only by the order parameter m in Eq. (45) would

be regular around the M I transition. However, as we will see below, this expansion has a piecewise analytic form in the metallic and insulating phases separately with a jump of the expansion coefficient at the transition point. This somewhat unconventional form of expansion is derived from the fact that some of the expansion coefficients explicitly depend on the density of states at the Fermi level, which has a discontinuity at the M I transition. This free-energy structure with a jump is in a complete contrast with the GLW form.

In this section, we consider the band-width control transition at half filling ($n = 1$) in the canonical ensemble. In the scheme of the canonical ensemble, we add a term n to the free energy defined in Eq. (45). The Hartree-Fock free energy F_{CHF} is given by

$$F_{CHF} = \frac{2T}{N_s} \sum_{k; \uparrow} \log[1 + \exp(-\frac{E(k)}{T})] + \frac{2}{2g} + n; \quad (50)$$

where $\sum_{k; \uparrow}$ runs over \uparrow and \downarrow . Hereafter, we describe F_{CHF} as F .

A. Free-energy expansion

Since dependence of F is explicitly given in Eq. (50), it allows a formal expansion of F in terms of Y around a nonzero value Y_c , by taking an expansion parameter $Y = Y_c + \delta Y$. The region $Y > 0$ ($Y < 0$) represents the metallic phase (insulating phase), respectively. The form of expansion is given as

$$F(Y) = F(Y_c) + AY + \frac{B}{2!}Y^2 + \frac{C}{3!}Y^3 + \dots; \quad (51)$$

where the coefficients are given by

$$A = \frac{\partial F}{\partial Y} \bigg|_{Y_c} = \frac{1}{g} W_1(Y_c); \quad (53)$$

$$B = \frac{\partial^2 F}{\partial Y^2} \bigg|_{Y_c} = \frac{1}{N_s} \sum_{k; \uparrow} \frac{\partial^2 f(E(k; \uparrow))}{\partial Y^2} \bigg|_{Y_c} W_2; \quad (54)$$

$$C = \frac{\partial^3 F}{\partial Y^3} \bigg|_{Y_c} = \frac{1}{N_s} \sum_{k; \uparrow} \frac{\partial^3 f(E(k; \uparrow))}{\partial Y^3} \bigg|_{Y_c} 3W_3; \quad (55)$$

with the definitions

$$W_1 = v_1; \quad (56)$$

$$W_2 = v_1 \frac{2}{c} v_3; \quad (57)$$

$$W_3 = v_3 \frac{3}{c} v_3; \quad (58)$$

Here, v_n is defined by

$$v_n = \frac{1}{N_s} \sum_{k; \uparrow} \frac{\partial^n f(E(k; \uparrow))}{\partial Y^n} \bigg|_{Y_c}; \quad (59)$$

To derive Eqs. (54) and (55), we neglect terms those are proportional to

$$\frac{\partial f(E(k; \uparrow))}{\partial Y} \bigg|_{Y_c} \frac{\partial}{\partial Y} \left(\frac{1}{1 + \frac{2}{c}} \right); \quad (60)$$

because of the following reason: At $T = 0$, this term has nonzero value only at $E(k; \uparrow) = 0$ (on the Fermi surface) because $\partial f(E(k; \uparrow)) / \partial Y = \delta(E(k; \uparrow))$ becomes the delta function. At the M I transition point, since the Fermi energy has the same value as that of the top [bottom] of the lower [upper] band, $\partial f(E(k; \uparrow)) / \partial Y = \delta(E(k; \uparrow) - E_c)$ has nonzero value only at $(k; \uparrow) = (k; 0)$, respectively. However, at the M I transition point, namely at $(k; \uparrow) = (k; 0)$ and $(k; \downarrow) = (k; 0)$, $\frac{1}{1 + \frac{2}{c}} = 0$ is satisfied, then $\frac{\partial f(E(k; \uparrow))}{\partial Y} \bigg|_{Y_c} \frac{\partial}{\partial Y} \left(\frac{1}{1 + \frac{2}{c}} \right)$ becomes zero. From this, the term defined in Eq. (60) vanishes at the M I transition point Y_c at $T = 0$.

Next, we derive more explicit forms of coefficients B and C at $T = 0$. We first consider the contribution of the first term of Eq. (54) and (55) at $T = 0$. The first term of Eq. (54) is given by

$$\begin{aligned} & \frac{1}{N_s} \sum_{k; \uparrow} \frac{\partial^2 f(E(k; \uparrow))}{\partial Y^2} \bigg|_{Y_c} \frac{\partial}{\partial Y} \left(\frac{1}{1 + \frac{2}{c}} \right) \\ &= \sum_{k; \uparrow} \int dE D(E) G(T; E) \\ &= \frac{c}{1 + \frac{2}{c}} + \sim \frac{c}{1 + \frac{2}{c}}; \end{aligned} \quad (61)$$

where $D(E)$ is the density of states of the upper (lower) band for $\uparrow = +1$ (-1), respectively, \sim is a cut-off and $G(T; E)$ is defined by

$$G(T; E) = \frac{\exp(-E/T)}{T(1 + \exp(-E/T))^2}; \quad (62)$$

We introduce a constant \sim for the linear coefficient between Y_c and Y as

$$\sim = \sim(Y_c) \frac{2}{c} T; \quad (63)$$

Detailed derivation of \sim at $T = 0$ is described in Appendix B. Explicit form of \sim at $T = 0$ is given by

$$\sim = \frac{2t^0}{2t^0 + \frac{t^2}{t^2}}; \quad (64)$$

The function $G(T; E)$ becomes the delta function at $T = 0$. Then, Eq. (61) is discontinuous at the M I transition at $T = 0$, because the density of states at the Fermi level is

discontinuous between the metallic and insulating sides. In fact, at $T = 0$, we obtain the relation

$$(61) : \begin{cases} = (D_+ (1 + \sim) + D_- (1 - \sim)) & \text{for } Y > 0 \\ = 0 & \text{for } Y < 0 \end{cases}$$

where D_+ (D_-) is the density of states at the bottom (top) of the upper (lower) band, respectively. Explicit forms of D_+ and D_- are given by

$$D_+ = \frac{1}{4t^0} \quad (65)$$

$$D_- = \frac{1}{2} \frac{1}{t^2} : \quad (66)$$

Detailed derivation of D_+ and D_- are given in Appendix B.

Using the similar derivation, we obtain the representation of the first term of Eq. (55) as

$$\begin{aligned} X &= \int dE D(E) \frac{\partial G(T; E)}{\partial E} \\ &= \frac{1}{2} \frac{1}{t^2} + \sim \quad (67) \end{aligned}$$

From this, we obtain the relation as

$$(67) : \begin{cases} = (1 + \sim)^2 R_+(T) + (1 - \sim)^2 R_-(T) \\ + \frac{Q_+(T)}{c} (1 + \sim) (3 + \sim) \\ + \frac{Q_-(T)}{c} (1 - \sim) (3 - \sim) & \text{for } Y > 0 \\ = 0 & \text{for } Y < 0 \end{cases}$$

where $R_+(T)$ and $Q_+(T)$ are defined by

$$R_+(T) = \int dE \frac{\partial D_+(E)}{\partial E} G(T; E) \quad (68)$$

$$Q_+(T) = \int dE \frac{D_+(E)^2}{D_+(E)} G(T; E) : \quad (69)$$

Finally, at $T = 0$, we obtain the free-energy expansion for metallic and insulating sides as

$$F = AY + \frac{B_m}{2!} Y^2 + \frac{C_m}{3!} Y^3 : : : ; \quad (70)$$

$$F = AY + \frac{B_i}{2!} Y^2 + \frac{C_i}{3!} Y^3 : : : ; \quad (71)$$

where

$$A = \left(\frac{1}{4} W_1 \right)_c \quad (72)$$

and the coefficients of the metallic side ($< c$) are given as

$$B_m = W_2 - ((1 + \sim)D_u + (1 - \sim)D_l) + \frac{1}{g} \quad (73)$$

$$\begin{aligned} C_m = & 3W_3 - R_+(0) (1 + \sim)^2 + R_-(0) (1 - \sim)^2 \\ & + \frac{Q_+(0)}{c} (1 + \sim) (3 + \sim) + \frac{Q_-(0)}{c} (1 - \sim) (3 - \sim); \end{aligned} \quad (74)$$

and the coefficients of the insulating side ($> c$) are given as

$$B_i = W_2 + \frac{1}{g} \quad (75)$$

$$C_i = 3W_3 : \quad (76)$$

We emphasize that, while A is common, the coefficients B and C in the region $Y > 0$ have values different from that in the region $Y < 0$ at $T = 0$. Although the coefficients B and C jump at $Y = 0$, F is regular (namely, piecewise analytic) within each region $Y > 0$ and $Y < 0$. Then the Taylor series expansion (70) as well as (71) is allowed in each sector $Y > 0$ and $Y < 0$ separately and they are unique. The coefficient C_i is negative if t^0 is not too large, because the sign of W_3 is determined from the dominant contribution proportional to v_3 , which has the positive sign due to the contribution from the lower band dominating over the upper-band contribution. On the other hand, C_m is positive for the relevant region of t^0 , namely for not too large value of $|t^0|$, because the dominant contribution is then from the term proportional to Q_+ . Therefore, the M I transition takes place in the parameter regions of $C_m > 0$ and $C_i < 0$, which makes F always bounded from below within the expansion up to the cubic order of Y . In fact, we will show below that the expansions up to the cubic order is enough for the purpose of deriving critical properties. Note that this expansion up to the cubic order is consistent with that obtained in the scaling theory and its phenomenological extension for two-dimensional systems [36, 37, 38]. We will show below that the universality class obtained in the present paper by the microscopic Hartree-Fock calculation indeed agrees with the prediction of the scaling theory and further reveals a microscopic mechanism of the emergence of the unconventional universality.

The carrier density X , which is the sum of the electron density X_- and the hole density X_+ in the metallic phase near M I transitions, is given as

$$X = X_+ + X_- = \frac{1}{c} (1 + \sim) Y : \quad (77)$$

Details of the derivation of Eq. (77) are given in Appendix A. Since X is proportional to Y in the metallic phase, the singularity of X is the same as that of Y . Therefore, whichever of X or Y is taken as the order parameter, the critical exponents are the same in the metallic side.

B. Critical exponents

Using the free-energy expansion obtained in the previous subsection, we are able to obtain the critical exponents of the quantum M I transitions.

Phase diagram of the M I transitions in the A - B_m plane is shown in Fig. 4 for the region close to $A = B_m = 0$. Metallic states are realized when the minimum is at a

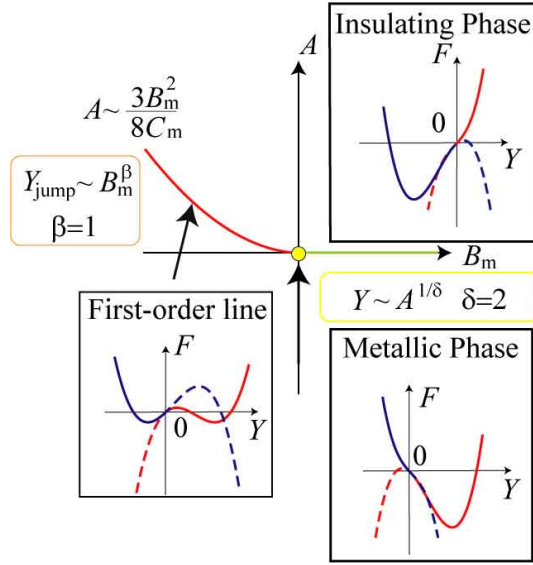


FIG. 4: (color online) Phase diagram in A - B_m plane. The first-order transition line is given by the condition $A = 3B_m^2/8C_m$ with $B_m < 0$, which separates the metallic phase $A < 3B_m^2/8C_m$ from the insulating phase in the other side. For $B_m > 0$ the transition becomes continuous and the transition line is given by $A = 0$ (see Eq. (96)). Typical Y dependence of the free energy along the first-order transition line, in the metallic and insulating phases are also shown in the insets. The definition of the free energy is given in Eqs. (70) and (71). The real Y dependence of the free energy is represented by the solid lines, where the metallic (insulating) side corresponds to the region $Y > 0$ ($Y < 0$), respectively. Broken lines represent the behaviors of Eqs. (70) and (71) extrapolated to the other sides $Y < 0$ and $Y > 0$, respectively. For the derivation of the phase boundary, see the text.

positive Y_m , whereas insulating states are stabilized when the minimum is at a negative Y_i . From Eq. (51), a local minimum appears at

$$Y_m = \frac{B_m + \frac{P}{B_m^2} - \frac{2AC_m}{C_m}}{C_m}; \quad (78)$$

if $B_m^2 > 2AC_m$ and at

$$Y_i = \frac{B_i + \frac{P}{B_i^2} - \frac{2AC_i}{C_i}}{C_i}; \quad (79)$$

if $B_i^2 > 2AC_i$ is satisfied. Because F is bounded from below, there always exists the absolute minimum either in the region $Y_i \leq 0$ or $Y_m \leq 0$. The location of the absolute minimum and the phase boundary shown in Fig. 4 are clarified below by classifying the parameter values into several cases. Then the critical exponents are derived in each region. We remind that $B_i > B_m$ and $C_i < 0 < C_m$ are always satisfied in all the relevant regions.

1. Quantum critical line

The continuous M-I transition line (quantum critical line) is determined from the condition $A = 0$ and $B_m > 0$. Along this quantum critical line, the free-energy minimum exists at $Y = 0$. For nonzero A near the quantum critical line $A = 0$, Eqs. (78) and (79) are reduced to

$$Y_m = \frac{A}{B_m} \quad (80)$$

and

$$Y_i = \frac{A}{B_i}; \quad (81)$$

respectively. Because the coefficient A plays the role of the conjugate field to Y , the critical exponent is defined from the growth of Y for small but nonzero A as

$$Y \sim A^{1/\delta}; \quad (82)$$

Therefore, $\delta = 1$ is obtained in both of the metallic and insulating sides.

The susceptibility in the metallic and insulating phases are given by

$$\begin{aligned} \chi_m &= \frac{d^2 F}{d(Y)^2} \bigg|_{Y=Y_m} = \frac{1}{B_m}; \\ \chi_i &= \frac{d^2 F}{d(Y)^2} \bigg|_{Y=Y_i} = \frac{1}{B_i}; \end{aligned} \quad (83)$$

respectively. Along the quantum critical line, B is of course always positive for the region $B_m > 0$ in whichever of the insulating and metallic sides. Therefore, the susceptibility does not diverge and the critical exponent defined by

$$\chi \sim A^{-\gamma} \quad (84)$$

is given as

$$\gamma = 0; \quad (85)$$

As we mentioned in Eq. (14) in Sec. I, the critical exponent does not represent the singularity of the specific heat in the case of the quantum phase transition. It rather characterizes the singularity of $\chi = \partial^2 F / \partial A^2$, because in the present case around the quantum critical line, $A \propto g - g_c$ holds. Near the quantum critical line of the M-I transition, the free energy F at the minimum is scaled by A as

$$F \sim A^2; \quad (86)$$

as is shown by substituting Eqs. (80) and (81) into Eqs. (70) and (71). From Eq. (14), this indicates $\gamma = 0$. The exponent is not well defined on the quantum critical line [51], because it is not possible to control the parameter g to cause the phase transition without applying the field A conjugate to the order parameter.

The free energy form (70) and (71) with nonzero A , B_m and B_m is equivalent to the case of the transition between metals and band insulators for noninteracting electron systems, if one replaces Y with the carrier density X of noninteracting electrons. By utilizing the equivalence with this noninteracting system, in the present case of the quantum critical line, we also obtain $\chi \sim X^{-1/2} / \omega$ leading to $\gamma = 1/2$. On the other hand, one can also calculate the dynamical susceptibility of the carrier density in the noninteracting system, which yields $\chi = S / E_F^{-1} / k_F^2 / \omega^2$. Here, E_F is the Fermi energy. This leads to the dynamical exponent $z = 2$.

Now we summarize the critical exponents on the quantum critical line: $\gamma = 0$; $\beta = 0$; $\nu = 1$; $\gamma = 1/2$ and $z = 2$. This is common to both of the insulating and metallic sides of the transition.

2. Marginal quantum critical point

When B_m becomes zero, the quantum critical line terminates at the marginal quantum critical point (MQCP) and the first-order transition boundary starts. Around MQCP, we show that the exponents depend on the approach to the critical point either from the metallic side or from the insulating side. To clarify such route dependence, we introduce four routes to approach MQCP as is illustrated in Fig. 5.

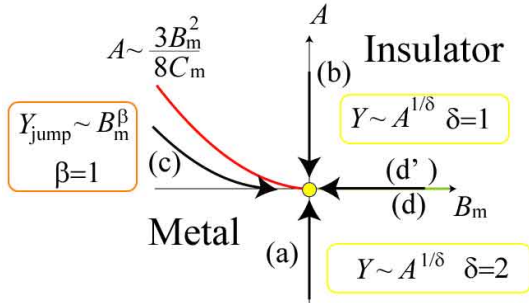


FIG. 5: (color online) Four routes to approach MQCP. Solid line in the negative B_m region represents the first-order transition line. The quantum critical line is given by the condition $A = 0$ and $B_m > 0$ (see text). Route (a) is the way to approach MQCP by controlling the external field A from the metallic region. The singularity of the Y along the route (a) is characterized by the critical exponent β . Route (b) is the way to approach MQCP from the insulating phase. Route (c) is the way to approach MQCP along the first-order transition line $A \sim \frac{3}{8} B_m^2$ as is derived in Eq. (96). Route (d) [(d')] is the way to approach MQCP along the quantum critical line from the metallic [insulating] phase.

From the free-energy expansion, the coefficient A represents the conjugate field to the order parameter and B represents the control parameter g . Therefore, we obtain the critical exponent through the route (a) or (b) in the following:

Route (a)

In the metallic side, through the route (a) in Fig. 5, the coefficient A approaches zero by keeping $B_m = 0$. From Eq. (78), neglecting B_m , we obtain the singularity of Y as

$$Y_m \sim \frac{S}{C_m} \frac{2A}{j} \frac{1}{j} : \quad (87)$$

Therefore, the critical exponent in the metallic side is $\gamma = 2$: (88)

Note that this exponent is consistent with the value obtained in the scaling theory [2, 3, 36, 37, 38] as well as with that in the quantum Monte Carlo study [29, 30, 31].

The dynamical exponent of the present transition can be calculated from the correlation functions of the order parameter X . Namely, from the equal-time structure factor S for the carrier density X defined in Eq. (34) and the susceptibility defined in Eq. (35), z is given from Eq. (6). By calculating S and χ , we obtain $z = 4$ [50]. Alternatively, we can derive z from the following arguments: Characteristic length scale of the MI transitions is given by the mean carrier distance ℓ , which diverges at the continuous MI transition point including MQCP. Then, in two dimensions, carrier density X is proportional to ℓ^{-2} . The equal-time structure factor S has the same scaling ℓ^{-2} by its definition. On the other hand, from $\gamma = 2$, the susceptibility of the carrier density is scaled by X^{-1} / ω^2 . Then the dynamical critical exponent z is determined from the condition

$$\frac{S}{\chi} \sim \omega^{-z}; \quad (89)$$

as $z = 4$. It also yields that χ has the singularity $\chi \sim \omega^{-4}$ with $\gamma = 1/2$. The large dynamical exponent $z = 4$ is consistent with the previous predictions obtained beyond the mean-field approximations [2, 3, 30, 31].

The origin of such an unusually large z is now clarified from the present study: The dynamical exponent normally expresses the dispersion of quantum dynamics. Namely, one might expect that the carrier dynamics would be described by the dispersion $\omega \sim k^4$. However, this contradicts the quasiparticle dispersion (44), which is generically proportional to k^2 . This puzzle is solved when we realize that the gap amplitude decreases with the increase of carrier number. Because of this reduction of the gap, when the carrier density is fixed, the upper (lower) band edge as well as the Fermi level becomes lower (higher) than that we might expect from the rigid band picture obtained from the quasiparticle dispersion of insulators. Because of this self-consistent reduction of the gap, the Fermi level does not move as quickly as k^2 with increasing X and is rather pinned near the original band edge even when the carrier number increases. This results in an effectively flat dispersion and actually a higher exponent with $z = 4$ comes out. This is an intuitive picture for the filling-control transition. For the case

of the band-width control, where the chemical potential is fixed rather than the filling, the reduction of the gap further allows more electrons and hole carriers, which is again interpreted by an effectively attractive dispersion.

Route (b), (d⁰)

In the insulating phase, through the route (b) and (d⁰) in Fig. 5, only A becomes zero while B_i remains nonzero and positive even at MQCP. This condition generates the same criticality as that of the quantum critical line. Therefore, we obtain the critical exponents $\nu = 0$, $\beta = 1$, $\gamma = 0$ and $z = 2$.

Route (c)

Next we consider the critical exponent defined by

$$Y_{\text{jump}} \propto \beta_m j; \quad (90)$$

where Y_{jump} is the jump of Y across the first-order transition line located in the region $B_m < 0$. Near MQCP, from Eqs. (78) and (79), Y_{jump} is given by

$$Y_{\text{jump}} = \frac{Y_m - Y_i}{C_m} = \frac{\beta_m j}{C_m} + \frac{A}{B_i}; \quad (91)$$

where we define $\beta_m j = \frac{Y_m - Y_i}{C_m}$. From this definition, it turns out that $\beta_m j$ is of order unity. On the first-order transition line, the free energy in the metallic phase has the same value as that of the insulating phase, namely

$$F(Y_m) = F(Y_i); \quad (92)$$

Equation (92) leads to

$$\frac{A}{C_m} \beta_m j + \frac{B_m (\beta_m j)^2}{2C_m^2} + \frac{C_m (\beta_m j)^3}{6C_m^3} = \frac{A^2}{2B_i^2}; \quad (93)$$

Near MQCP, $\beta_m j$ and B_i are always nonzero and have amplitudes of the order unity. We assume that, for small quantities A and B_m , A has the order ν_1 and B_m has the order ν_2 . From Eq. (93), the relation between ν_1 and ν_2 is given by

$$O(\nu_1)O(\nu_2) + O(\nu_2^3) = O(\nu_1^2); \quad (94)$$

From this, to satisfy Eq. (93), the relation between ν_1 and ν_2 should be

$$\nu_1 = \frac{2}{2}: \quad (95)$$

Substituting Eq. (93) into Eq. (78) leads to $\nu = 3/2$. Namely, on the first-order transition line near MQCP, the relation between A and B_m should be

$$A \propto \frac{3B_m^2}{8C_m}; \quad (96)$$

Using this relation, near MQCP, the singularity of Y_{jump} is given by

$$Y_{\text{jump}} \propto \frac{3B_m^2}{8C_m B_i} + \frac{3\beta_m j}{2C_m} / \beta_m j; \quad (97)$$

Therefore, the critical exponent is given by

$$\nu = 1; \quad (98)$$

Route (d)

The route (d) along the quantum critical line ($A = 0$ and $B_m > 0$) always keeps $A = 0$. Although the susceptibility remains finite on the quantum critical line itself ($\nu = 1/B_m$), the amplitude $1/B_m$ increases toward MQCP and it diverges in the limit to MQCP because of $B_m \rightarrow 0$. The singularity of the susceptibility

$$\chi \propto j^{-\gamma} \quad (99)$$

is given by

$$\chi = \frac{d^2 F}{d(Y)^2} \propto \frac{1}{\beta_m j^2} / j^{-\gamma} j^{-1}; \quad (100)$$

Therefore, in the metallic phase, the susceptibility diverges at MQCP with the critical exponent

$$\nu = 1; \quad (101)$$

Near MQCP, the free energy F at the minimum in the metallic side is scaled by the control parameter B_m as

$$F \propto B_m^3; \quad (102)$$

For MQCP, $B_m \propto g^{-\nu_g}$ holds in contrast to $A \propto g^{-\nu_g}$ for the quantum critical line. Then from Eq. (14), we obtain the exponent $\nu = 1$. We remark again that ν has no direct relation with the singularity of the specific heat. In the insulating side, as mentioned above for the route (d⁰), $\nu = 0$ is obtained.

Now the critical exponents for MQCP are summarized as

$$\nu = 1; \quad \beta = 1; \quad \gamma = 1; \quad \nu = 2; \quad \nu = 1/2 \text{ and } z = 4 \quad (103)$$

for the metallic side and

$$\nu = 0; \quad \beta = 1; \quad \gamma = 0; \quad \nu = 1; \quad \nu = 1/2 \text{ and } z = 2 \quad (104)$$

for the insulating side. The scaling laws (15) and (16) as well as the hyperscaling Josephson relation (24) associated with the hyperscaling Eq. (9) are all satisfied in both of the two sides.

C. Crossover of the critical exponent

In the metallic region, Y grows from zero at MQCP when A and/or B_m deviate from zero. As a function of the distance from MQCP defined by $r = \sqrt{A^2 + B_m^2}$ in the A - B_m plane, Y grows as $Y \propto r$ for $A = 0$ because of Eq. (97) whereas it is scaled as $Y \propto r^{1/2}$ for $B_m = 0$ because of Eq. (87). Then a crossover between $Y \propto r$

and $Y / r^{\frac{1}{2}} m$ must exist. Here, we specify the location of this crossover boundary below.

Near MQCP, Y_m is given as

$$Y_m = \frac{B_m + \frac{p}{q} \frac{B_m^2 - 2A_m C_m}{C_m}}{B_m^0 + \frac{p}{q} \frac{B_m^0^2 + A_m^0}{C_m}} \quad (105)$$

$$= \frac{B_m^0 + \frac{p}{q} \frac{B_m^0^2 + A_m^0}{C_m}}{B_m^0 + \frac{p}{q} \frac{B_m^0^2 + A_m^0}{C_m}}; \quad (106)$$

where we define $B_m^0 = B_m = C_m$ and $A_m^0 = 2A = C_m > 0$. In the region where the condition $A_m^0 - B_m^0^2$ is satisfied, Y_m behaves as

$$Y_m = B_m^0 + \frac{p}{q} \frac{A_m^0}{A_m^{\frac{1}{2}}}; \quad (107)$$

This indicates that MQCP exponent ($= 2$) dominates in this region. In contrast, in the region where the condition $A_m^0 - B_m^0^2$ is satisfied, Y_m behaves as

$$Y_m = B_m^0 + B_m^0 \left(1 + \frac{A_m^0}{B_m^0^2}\right) \quad (108)$$

$$\frac{A_m^0}{B_m^0^2} / A_m^{\frac{1}{2}}; \quad (109)$$

From this, in this region the criticality of the quantum critical line represented by $\nu = 1$ dominates. In Fig. 6, the crossover line is represented by the broken line.

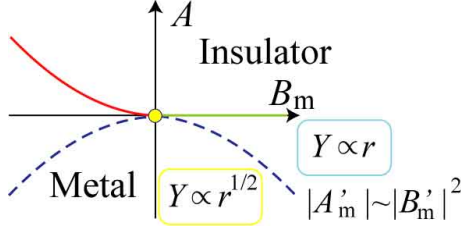


FIG. 6: (color online) Crossover line between the scaling region Y / r and $Y / r^{\frac{1}{2}}$, which is represented by the broken (blue) line defined by $A_m^0 - B_m^0^2$.

D. Location of marginal quantum critical point

From the free-energy form, the location of MQCP is determined by the condition

$$A = 0 \text{ and } B_m = 0; \quad (110)$$

The line $A = 0$ is determined by

$$= c; \quad (111)$$

with the definition $c = 2t^0$. From Eq. (111), the relation between g and t^0 for $A = 0$ is given, because ν is an implicit function of g and t^0 . We calculate B_m from Eq. (73) with the condition Eq. (111). We then find that B_m becomes zero at two points, namely two MQCPs exist at

zero temperature. Figure 7 shows numerical estimate of B_m near MQCP from Eq. (73).

From this, we estimate the location of MQCP at $t_c^0 = t = 0.05571$, $g_c = 0.616180$ and $t_c^0 = t = 0.36455$, $g_c = t = 1.38144$, respectively. We call MQCP at $t_c^0 = 0.05571$, MQCP₁ and MQCP at $t_c^0 = 0.36455$, MQCP₂, respectively.

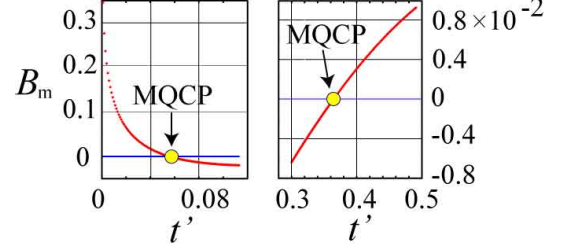


FIG. 7: (color online) Coefficient B_m on the line $A = 0$ ($= c$) near MQCP. We estimate the points $B_m = 0$ as $t_c^0 = t = 0.05571$, and 0.36455 . In the positive B_m region, the continuous MI transition occurs, while in the negative B_m region, the first-order MI transition occurs.

E. Finite temperature effect

In this subsection, we analyze how the free energy and critical properties are modified at nonzero temperatures. Since the discontinuity of the coefficient arising from the singularity of the density of states is immediately smeared out by the Fermi distribution at $T > 0$, the free-energy expansion should convert into the expansion of the conventional ν theory in the critical region. The universality class of MQCP then switches over to the Ising universality class. Here, we show how the expansion in Eq. (51) breaks down and the Ising critical region appears.

The discontinuity of the coefficient B and C comes from the integration of the form

$$P = \int_{-\infty}^{\infty} dE \frac{X}{D(E)H(E)G(T;E)}; \quad (112)$$

where $H(E)$ is a slowly varying function of E in the range $E = 0(T)$. Now the density of states $D_+(E)$ is nonzero only in the interval

$$(1 - \sim)Y < E < \sim; \quad (113)$$

whereas $D_-(E)$ is nonzero in the window

$$< E < (1 + \sim)Y; \quad (114)$$

The correction factor proportional to \sim arises from the chemical potential shift from the case of $Y = 0$. By considering Eq. (62), Eq. (112) is reduced to

$$P = 2H(0) \int_{-\infty}^{\infty} dE \frac{(1 + \tanh \frac{(1 - \sim)Y}{2T})}{D(E)}; \quad (115)$$

if the energy dependence of the density of states $D(E)$ can be ignored. Since $(1-\sim)=2$ and $(1+\sim)=2$ in Eq. (115) are the quantities of the order unity, from Eq. (112), for $Y \gg T$, P behaves similarly to that of the step function as shown in Fig. 8. Therefore, for $Y \gg T$, the expansion Eq. (51) is valid and the MQCP criticality appears. We call this region the quantum region. On the other hand, for $Y \ll T$, P behaves differently from that of the step function as shown in Fig. 8, and behaves as a smooth function of Y . Therefore, the expansion (51) breaks down and the conventional GLW expansion Eq. (3) becomes justified, where the Ising criticality appears. We call this region the classical region. We expect that fluctuations modify the mean-field exponents for the Ising universality because the upper critical dimension of the Ising universality is four. We do not go into detail on this point.

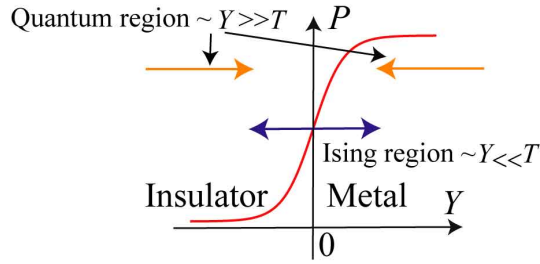


FIG. 8: (color online) Schematic behavior of P as function of Y . In $Y \gg T$ region P behaves as the step function and the expansion (51) is valid, while in $Y \ll T$ region P behaves as Fermi distribution function and the expansion (51) breaks down.

Now, we clarify width of the quantum region for each route shown in Fig. 9.

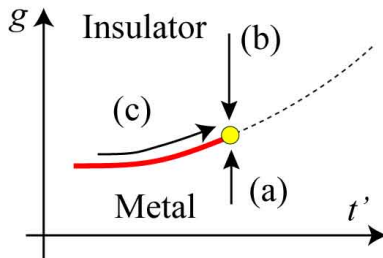


FIG. 9: (color online) Routes to the critical point in plane of g and t' at fixed temperature T . Solid thick (red) line represents the first-order transition line and it terminates at the finite-temperature critical point represented by the (yellow) circle. Route (c) is the way to the finite-temperature critical point along the first-order transition line with constant T . Routes (a) and (b) are the routes to the critical point with fixed temperature from the metallic and insulating phases, respectively. Broken line represents the crossover line, where dj/dg has the maximum value.

Route (a)

In the quantum region, the singularity of Y_m is given from Eq. (87) as

$$Y_m / \frac{A_j}{C_m} \sim a j^{\frac{1}{2}} g^{\frac{1}{2}}; \quad (116)$$

where a is a g -independent constant given by

$$a = \lim_{j \rightarrow 0} \frac{1}{j^{\frac{1}{2}} g^{\frac{1}{2}}} \frac{A_j}{C_m}; \quad (117)$$

From this, the condition of quantum region $Y \gg T$ is given by

$$j^{\frac{1}{2}} g^{\frac{1}{2}} \gg \frac{T^2}{a^2}; \quad (118)$$

Route (b)

In the quantum region, the singularity of Y_i is given by

$$Y_i / \frac{A}{B_i} \sim b j^{\frac{1}{2}} g^{\frac{1}{2}}; \quad (119)$$

where b is a g -independent constant defined by

$$b = \lim_{j \rightarrow 0} \frac{1}{j^{\frac{1}{2}} g^{\frac{1}{2}}} \frac{A}{B_i}; \quad (120)$$

From this, the condition of quantum region $Y \gg T$ is given by

$$j^{\frac{1}{2}} g^{\frac{1}{2}} \gg \frac{T}{b}; \quad (121)$$

Route (c)

In the quantum region, the singularity of Y_{jup} is given from Eq. (97) as

$$Y_{jup} / \frac{B_m j}{C_m} \sim c j^0 g^0; \quad (122)$$

where a g -independent constant c is defined by

$$c = \lim_{j \rightarrow 0} \frac{1}{j^0 g^0} \frac{B_m}{C_m}; \quad (123)$$

From this, the condition of quantum region $Y \gg T$ is given by

$$j^0 g^0 \gg \frac{T}{c}; \quad (124)$$

IV. NUMERICAL HARTREE-FOCK RESULTS AT $T = 0$

In this section, we show numerical results of MQCP obtained by numerically solving the Hartree-Fock self-consistent equation (46) itself without relying on the free-energy expansion (51). We will show that numerical results are consistent with the free-energy expansion in the previous section.

A . Phase diagram at zero temperature

We first present the phase diagram at $T = 0$ in Fig.10. We find two MQCPs in the phase diagram in agreement with the free-energy expansion.

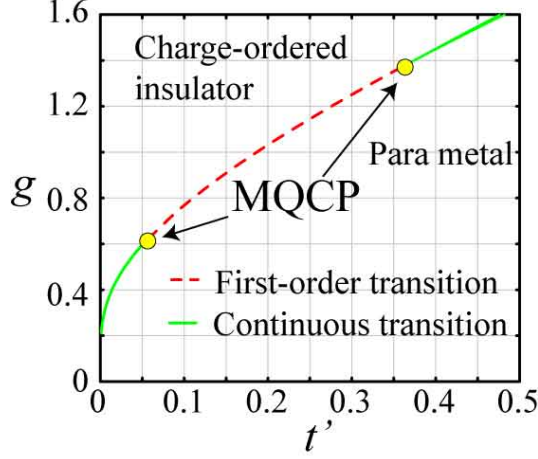


FIG. 10: (color online) Phase diagram at $T = 0$. Broken (solid) line represents the first-order (continuous) transition line, respectively. Near MQCP, charge-ordered metal appears. Detailed phase diagram near MQCP is shown in Figs. 11 (a) and 11 (b)

At $t^0 = 0$, the perfect nesting occurs and the charge ordered phase begins from $g = 0$. For a narrow window below the triple point ($t^0 = 0.085t$, $g = 0.694t$), charge-ordered metal (COM) appears between paramagnetic metal (PM) and charge-ordered insulator (COI) phases as is shown in Fig. 11 (a) in detail. The triple point represents the point where PM, COM and COI coexist. The order of the transitions from PM to COM is continuous, while the order of transition from COM to COI changes from the continuous to the first order with increasing $t^0 = t$. The continuous transition line between PM and COM terminates at the triple point. The quantum critical line between COI and COM terminates at MQCP₁ ($t^0 = 0.05571t$, $g = 0.6161t$).

For large t^0 region ($t^0 > 0.35t$), another triple point appears at $t^0 = 0.357t$, $g = 1.366t$ and COM appears between COI and PM as is shown in Fig. 11 (b) in detail. The quantum critical line between COM and COI terminates at MQCP₂ ($t^0 = 0.3645t$, $g = 1.381t$) again.

Figure 12 shows the jump of Y (Y_{jump}) as a function of t^0 across the first-order MI transition line at $T = 0$. The (red) squares and (purple) triangles show Y_{jump} between COM and COI and between COI and PM, respectively, as a function of t^0 . Y_{jump} vanishes at MQCP.

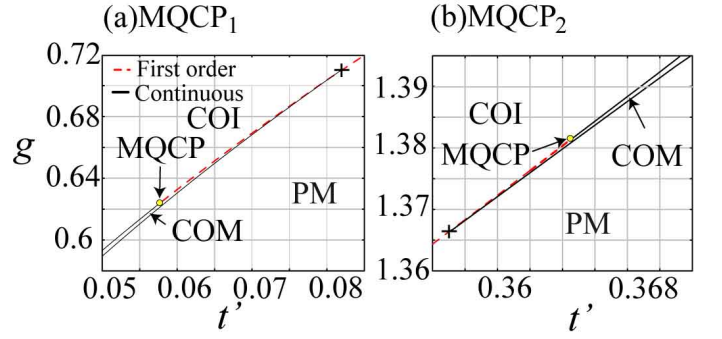


FIG. 11: (color online) (a) Phase diagram near MQCP₁ ($t^0 = 0.05571t$, $g = 0.6161t$). The continuous (first-order) transition is shown by the solid (broken) line, respectively. MQCP is shown by the circle, where the first-order transition line terminates. The cross point represents the triple point where COI, COM and PM coexist. (b) Phase diagram near MQCP₂ ($t^0 = 0.3645t$, $g = 1.381t$).

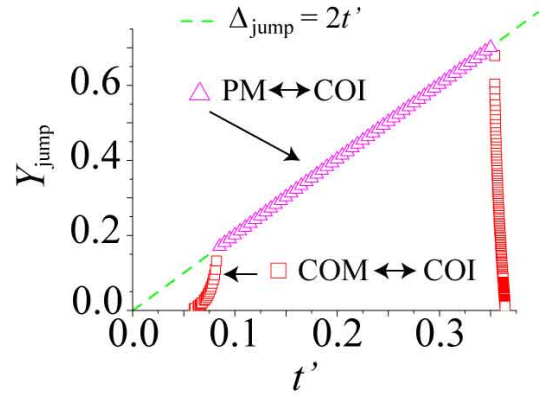


FIG. 12: (color online) Y_{jump} as a function of t^0 on the first-order MI transition line. For the first-order transition between PM and COI shown by triangles, Y_{jump} is slightly larger than $c = 2t^0$.

B . Critical exponents of MQCP

We clarify the singularity of Y near MQCP numerically. Hereafter, we only consider MQCP at $t_c^0 = 0.36455$, namely MQCP₂ through the route (a) (d) in Fig. 5. Critical exponents of MQCP₁ is the same as that of MQCP₂. We show that the numerical Hartree-Fock results are consistent with the results obtained by the free-energy expansion in the previous section.

Route (a)

First, we confirm that the critical exponent in the metallic region defined by

$$Y_m / A_j^{-1} \text{ and } Y_m \propto g_j^{-1} \quad (125)$$

is consistent with the value obtained by the free-energy expansion. We perform least square fitting for Y_m as

a function of $g_c - g$ near MQCP. Figure 13 shows the results of the least square fitting. We estimate the critical exponent as

$$\nu = 2.0001(6): \quad (126)$$

This is consistent with $\nu = 2$ obtained by the free-energy expansion. We estimate the coefficient a defined in Eq. (117) as

$$a = 13.48(4): \quad (127)$$

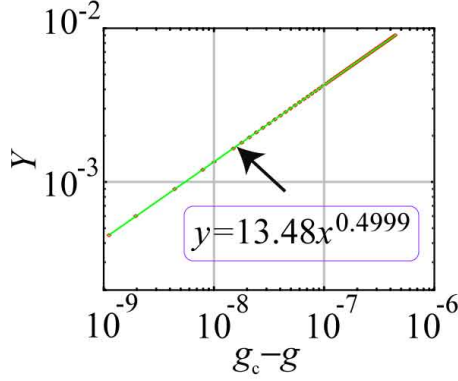


FIG. 13: (color online) Log-log plot of Y_m as function of $g_c - g$ at $t^0 = t = 0.36455$. Solid (green) line shows the result of least square fitting by assuming the function $y = ax^{1/\nu}$, where $y = Y_m$ and $x = (g_c - g)$. Results of least square fitting are given as $1/\nu = 0.49996(2)$ and $a = 13.48(4)$. Critical gap Δ_c is obtained as $\Delta_c = 2t^0 = 0.72911t$ and the critical interaction g_c is estimated as $g_c = 1.38144$.

Route (b)

We also obtain the critical exponent in the insulating region. The definition of ν is given by

$$Y_i / \beta_j^{-1} \text{ and } Y_m \propto \beta_j^{-1} g_j^{-1} \quad (128)$$

The numerically obtained critical exponent is

$$\nu = 1.000000(4): \quad (129)$$

The coefficient b defined in Eq. 120 is estimated as

$$b = 0.996429(4): \quad (130)$$

Now it was confirmed that the Hartree-Fock result is consistent with the exponent $\nu = 1$ obtained by the free-energy expansion.

Route (c)

Next, we consider the critical exponent defined by

$$Y_{\text{jump}} / \beta_m j / c j^0 \ell j: \quad (131)$$

We estimate the critical exponent as

$$\nu = 1.01(1): \quad (132)$$

This critical exponent is consistent with $\nu = 1$ obtained by the free-energy expansion. The coefficient c defined in Eq. (123) is estimated as

$$c = 35.2(1): \quad (133)$$

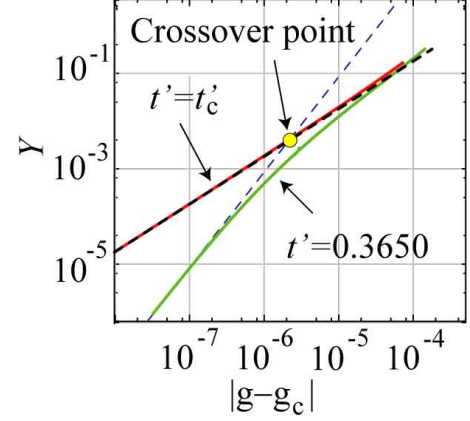


FIG. 14: (color online) Crossover points of the critical exponent determined from $g - g_c$ dependence of Y for $t^0 = 0.3650$ near MQCP₂ at $t^0 = 0.364555$. Away from the transition point, behavior of Y for $t^0 = 0.3650$ asymptotically approaches that of Y for $t^0 = 0.364555$. Crossover point is determined from the crossing point of a $\beta_j^{-1} g_j^{-2}$ and a $\beta_j^{-1} g_j$. The t^0 dependence of the crossover point is shown in Fig. 15.

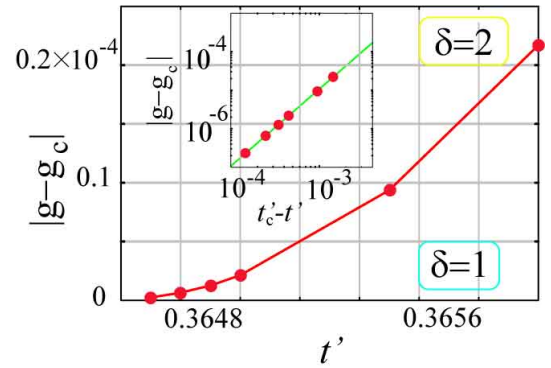


FIG. 15: (color online) Crossover boundary between $\nu = 2$ region and $\nu = 1$ region in plane of $g - g_c$ and t^0 . The inset shows log-log plot of crossover in plane of $\beta_j^{-1} g_j$ and $t_c^0 - t^0$. Solid (green) line shows the result of least square fitting near MQCP by assuming the function $y = kx^2$, where $y = \beta_j^{-1} g_j$ and $x = t_c^0 - t^0$.

C. Crossover of the critical exponent

The critical exponent has different values between the quantum critical line and MQCP and it may show a

crossover when the critical regions meet. Here, we show numerical results for the crossover of the critical exponent at $T = 0$. As already mentioned, at MQCP, singularity of Y is well fitted by the function $Y \propto g^{1/2}$ with $\delta = 2$ and $a = 13.48$. Away from MQCP, crossover from 2 to 1 near the quantum critical line. In Fig. 14, we show the least square fitting for g dependence of Y by assuming the function $Y \propto g^{1/3}$, where $\delta = 3$. The crossover point is estimated by the crossing point of the function $Y \propto g^{1/3}$ and $Y \propto g^{1/2}$, which is illustrated in Fig. 15. The inset in Fig. 15 shows that the t^0 dependence of the crossover point is well fitted by the function $f \propto t^{1/2}$. This is consistent with the analytical result.

V. NUMERICAL HARTREE-FOCK RESULTS AT $T = 0$

To understand quantitatively, we numerically study how critical exponents of MQCP cross over to those of Ising critical points by finite-temperature effects. As shown in the previous section, the free-energy expansion predicts that crossovers of the critical exponents depend on the routes (a)–(c).

Route (a)

In the metallic phase, we show the crossover of the critical exponent near the critical point for an example of $T = 0.001t$ in Fig. 16. Here, clearly crosses over from 2 (MQCP) to 3 (Ising mean-field value). We estimate the width of Ising region by the crossing point of two solid (green and blue) asymptotic lines. The value of g at the crossing point is denoted as g_c . The Ising region is given by $W < W_c$ for

$$W < g_c \quad (134)$$

and $W > g_c$. In the example in Fig. 16, the crossover occurs at

$$W_c = 0.6 \times 10^{-7}t. \quad (135)$$

On the other hand, the free-energy expansion in Eq. (118) indicates that the crossover is given by

$$W_{FE} = \frac{T^2}{a^2}t = \frac{0.001}{13.48^2}t = 10^{-8}t; \quad (136)$$

where a is estimated in Eq. (127). They are consistent each other.

For several choices of temperatures, the same analyses were performed and we determined the Ising region. We show the result in Fig. 17(a). In the free-energy expansion, the crossover W_c is expected asymptotically as $W_c \propto T^2$ at low temperatures. The scaling of W_c as a function of T appears to show somewhat smaller exponent p than two for the fitting $W_c \propto T^p$. The origin of this discrepancy is likely to come from temperature dependence in a . Except for this discrepancy, the order of

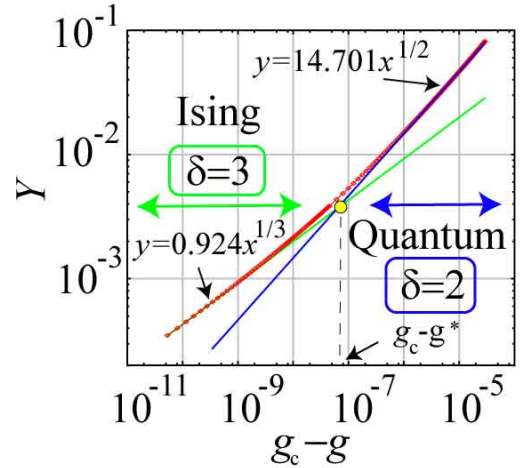


FIG. 16: (color online) Log-log plot of Y_m as function of $g_c - g$ near the critical point at $T = 0.001t$. Two thin solid (green and blue) lines show the results of least square fitting by assuming the function $y = ax^{1/3}$ and $y = a^0x^{1/2}$, respectively, where $y = Y_m$ and $x = g_c - g$. We obtain $a = 0.924(1)$ and $a^0 = 14.701(3)$.

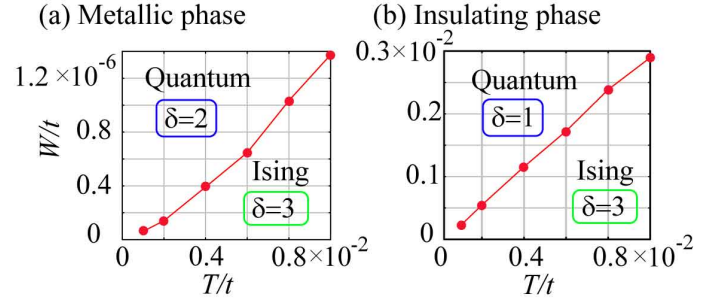


FIG. 17: (color online) (a) Phase diagram of crossover boundary between Ising and the quantum regions for in the metallic phase plotted in plane of $W = t$ and $T = t$. (b) Phase diagram of crossover boundary between Ising and quantum regions for in the insulating phase plotted in plane of $W = t$ and $T = t$.

the Ising region estimated from the Hartree-Fock calculations is consistent with that of the free-energy expansion.

Route (b)

In the insulating region, we show the numerically obtained phase diagram for the crossover in Fig. 17(b). To obtain the crossover point from $\delta = 3$ for the Ising region to $\delta = 1$ for MQCP, we have used a criterion different from the metallic side in the route (a). The slope of Y as a function of W is not a monotonic function of W and it crossovers first from $\delta = 3$ to an even smaller value, after which it increases to $\delta = 1$. To specify the crossover point, we have taken it as the point which shows the minimum slope in the crossover region. For example, at

$T = 0.001t$, W is estimated as

$$W = 2.23 \times 10^{-4}t; \quad (137)$$

The free-energy expansion indicates from Eq. (121) that the crossover point W for is given by

$$W_{FE} = \frac{T}{b} = \frac{0.001t}{0.99} \times 10^{-3}t; \quad (138)$$

where b is estimated in Eq. (130). As far as the order of W , it indicates that the Hartree-Fock numerical results are consistent with that of the free-energy expansion. Figure 17(b) is obtained by performing the same analyses for several choices of temperatures. The temperature dependence of the crossover is estimated as $W \propto T^{1.1}$. This is rather consistent with $W \propto T$ obtained from the free-energy expansion. It is likely that a slight discrepancy between two results comes from the temperature dependence of b .

Route (c)

We also discuss the crossover of the critical exponent in the route (c). For example, near the critical point at $T = 0.001t$, crosses over from 1 (MQCP) to $1/2$ (Ising mean-field) in a monotonic fashion. The crossover W is estimated by the same method as the route (a) as

$$W = 0.00037 \times 10^{-4}t; \quad (139)$$

In the free-energy expansion, the crossover is estimated from Eq. (124) as

$$W_{FE} = \frac{T}{c} = \frac{0.001t}{32.4} \times 10^{-4}t; \quad (140)$$

where c is estimated in Eq. (133). The numerical Hartree-Fock result is consistent with W_{FE} .

Figure 18 shows W at the crossover for several choices of temperatures. The temperature dependence of Ising region is estimated as $W \propto T^{0.7}$, which has somewhat smaller slope than $W \propto T$ expected from the free-energy expansion. Again, it is likely that the discrepancy comes from the temperature dependence of c . Numerical results suggest that we need to consider the overall temperature dependences of a , b and c on the quantitative level. However, we do not go further into details on this point. At least the existence of two critical regions governed by MQCP and Ising classes is now well established with crossovers, which are qualitatively consistent with the free energy expansion. The numerical results show how the asymptotic scaling for the location of the crossover derived in the free energy expansion are modified in regions distant from the critical point.

VI. COMPARISON WITH EXPERIMENTAL RESULTS

In real materials, strictly speaking, well defined Mott critical point has been observed so far only at finite temperatures, as we discuss below. There, Ising critical exponents should be observed in the region sufficiently close to

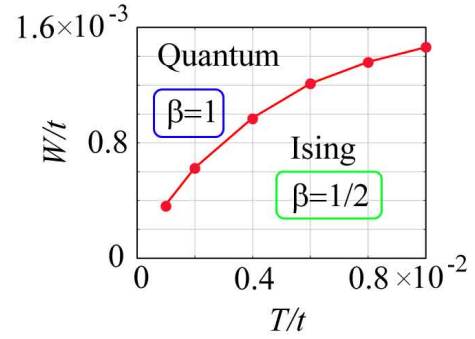


FIG. 18: (color online) Crossover boundary for the critical exponent plotted in plane of $W = t$ and $T = t$.

the finite-temperature critical point. However, because the Ising region is not wide enough at low temperatures and crosses over to MQCP criticality, quantum critical exponents may be observed in actual experiments. Although we have to be careful in comparing our results for the very simple model with possible artifact of the Hartree-Fock approximation with experimental results on more complicated systems, it may offer an insight into the relevance of the quantum criticality. Here, we compare our results with the experimental results of $-(\text{ET})_2\text{Cu}[\text{N}(\text{CN})_2]\text{Cl}$ reported by Kagawa, Miyagawa and Kanoda [46]. The critical exponents in the metallic phase show a clear evidence of the crossover in our numerical results for and . At $T_c = 0.01t$ (see Fig. 17(a)), the classical Ising region is observed for $W < 10^{-6}t$. This critical temperature is comparable to the experimental value $T_c \approx 40\text{K}$ with the estimated transfer $0.1\text{--}0.2\text{ eV}$ obtained from the Hückel calculation [52]. In $-(\text{ET})_2\text{Cu}[\text{N}(\text{CN})_2]\text{Cl}$, 1.0MPa roughly corresponds to $0.001t$ [52, 53], which is estimated from the pressure dependence together with the dependence on the anion species in the experimentally obtained phase diagram. The smallest distance from the critical point accessible in the experimental resolution is estimated as $P - P_{c,j} \approx 0.1\text{MPa} \times 10^{-4}t$, which is much larger than $10^{-6}t$ suggested from the theoretical estimate above. This indicates that, in the experiments, the distance between the true critical point and the available point closest to it is two orders of magnitude larger than the distance of the crossover boundary from the critical point. This is consistent with the experimental result that the singularity of the conductivity is well fitted only by the quantum critical exponent $\nu = 2$. Other exponents in this $-(\text{ET})$ compound shows $\nu = 1$ and $\nu = 1$. These are completely consistent with the present MQCP universality.

We have also obtained that in the insulating phase shows a crossover. The critical exponent changes into $\nu = 3$ (Ising) from $\nu = 1$ (MQCP). We estimate the Ising region as $W < W \times 10^{-3}t$ for $T_c = 0.01t$. This W corresponds to about 1.0MPa by assuming that 1.0MPa corresponds to $0.001t$. The Ising region in the insu-

lating phase is much wider than that of the metallic phase. From this, we have more chance for observing the Ising region ($\nu = 3$) in the experiments. The experimental result shows that effective charge gap closes with the singularity as $(P_c - P)^{0.4 \pm 0.1}$ in the insulating phase. This indicates that $\nu = 3 \pm 2$. This critical exponent may be consistent with the Ising mean-field value $\nu = 3$. If one were able to approach the Ising critical region ($P - P_c \sim 10 \text{ MPa}$) in the organic conductor of -ET compound, since the system is quasi-two-dimensional, the 2D Ising critical exponent $\nu = 15$ should be obtained. It could show a crossover from the quantum exponent $\nu = 1$ governed by MQCP to the Ising mean-field value $\nu = 3$ in the region closer to the critical point with an extremely narrow critical region of $\nu = 15$. However, since the experimental data are obtained in the parameter space not close enough to the Ising region of the critical point, the mean-field critical exponent may be obtained similarly to the case of $(\text{V}_{1-x}\text{Cr}_x)_2\text{O}_3$ [44]. Although the pressure dependence of the parameter value for the transfer is so far not available, high critical temperature $\sim 450 \text{ K}$ of $(\text{V}_{1-x}\text{Cr}_x)_2\text{O}_3$ likely enables the observation of the Ising criticality.

As we mentioned in Sec. I, some of the high- T_c cuprates such as $\text{Bi}_2\text{Sr}_2\text{CaCu}_2\text{O}_{8+y}$ and $(\text{La,Sr})_2\text{CuO}_4$ show consistency with $\nu = 2$, whereas some of other compounds such as $(\text{Ca,Na})_2\text{CuO}_2\text{Cl}_2$ shows a quicker shift, rather consistently with $\nu = 1$. This variety suggests that parameter values of various copper oxides correspond to a diverse range from the region close to MQCP to that deeply in the quantum critical line. The normal state properties as well as superconducting transition temperatures may depend on the distance from MQCP, which is an intriguing issue left for the future. In the case of filling-control transitions, the first-order transition appears as an intrinsic instability to the phase separation. The phase separation is transformed to the electronic inhomogeneity with finite-size domains under the constraint of the long-range Coulomb interaction and the charge neutrality. The distance from MQCP directly measures the tendency for the instability toward such inhomogeneities. The diversity of the cuprate superconductors in terms of this tendency can be classified by this distance.

^3He adsorbed on a graphite surface offers a unique purely two-dimensional fermion system. In addition to the anomalous suppression of T_F that is consistent with $z = 4$ [41] as mentioned in Sec. I, recent detailed study at lower temperatures has revealed richer structure in the specific heat [4]. The second layer of He approaches the registered phase (namely, a solid phase with commensurate periodicity to the first-layer solid at the density $4/7$ in terms of the first layer density) with increasing He pressure. Near but below the density at the registered phase, the lower temperature structure of the specific heat suggests that the large residual entropy expected from the large dynamical exponent $z = 4$ is released below 10 mK . A strong crossover around 10% doping be-

tween low and high density regions is suggested from the transfer of the entropy release, where the release from the specific-heat peak structure at $10\text{--}100 \text{ mK}$ for the lower density (more than 10% doping) region is replaced with the release at lower temperatures around or less than 1 mK for the higher density (less than 10% doping). The release at this low temperature region may arise from the superposition of the contribution from carrier motion and spin, which are originated from two different regions of Brillouin zone, respectively, as analyzed by the electron differentiation in momentum space with a simplified two-fluid picture [6]. This transfer of the entropy-releasing temperature implies a drastic topological change of the Fermi surface in the ground state such as Lifshitz transition to the small Fermi pocket or approximate arc structure. If a clear Lifshitz transition occurs, we expect a singular dependence of thermodynamic properties on the density measured at low temperatures below 1 mK . Another conceivable case is that such a singular dependence is not observable when the topological change occurs in the pseudogap region with faint spectral weight out of the "arc". This may be analyzed by measuring the data at temperatures lower than 1 mK in more detail around this crossover, which is an intriguing issue left for future studies. If Lifshitz transition occurs, the transition to the registered phase occurs also as a topological transition with vanishing Fermi pockets to the registered phase. So far, it is not clear whether the transition to the registered phase is eventually realized across the quantum critical line or near MQCP, because the lower temperature data below 0.1 mK is not available.

Physics of electron differentiation tightly associated with the present unusual universality of metal-insulator (or liquid-registered phase) transitions is a common central issue of the high- T_c cuprates and monolayer ^3He . The overall experimental indications show the relevance of the unusual quantum criticality around MQCP. More detailed analysis is left for future studies. Studies on the crossover effect beyond the Hartree-Fock approximation are also left for future studies.

VII. SUMMARY AND DISCUSSION

Quantum MI transitions between symmetry broken metals and insulators have been studied within the Hartree-Fock approximation using the extended Hubbard model. By increasing the onsite Coulomb interaction U and nearest-neighbor Coulomb interaction V , this model at half filling has a tendency to charge ordering or antiferromagnetic ordering within the mean-field level. Pre-existing gaps generated by such spontaneous symmetry breakings allow us to capture the essence of electron correlation effects on metal-insulator transitions. In this paper, we have mainly considered the case of the charge ordering in the region $4V > U$. However, it is essentially the same for the antiferromagnetic ordering in the region $U > 4V$ and the present study can be easily extended,

where the criticality does not change.

Using the Hartree-Fock free energy, we have studied the criticality of M I transitions. To clarify the nature of M I transitions, we have performed the free-energy expansion as

$$F = F(\phi_c) + AY + \frac{B}{2!}Y^2 + \frac{C}{3!}Y^3; \quad (141)$$

in terms of the gap amplitude measured from the M I transition point, $Y = \phi - \phi_c$. This free-energy expansion has an unconventional feature, where the coefficients B and C have different values between B_m and C_m in metals and B_i and C_i in insulators with jumps at the transition point $Y = 0$. Although the expansion is not regular at $Y = 0$, Y dependence of F is regular in a piecewise analytic way in each metallic ($Y > 0$) and insulating ($Y < 0$) region separately, which makes the expansion unique. Because of the jump from $C_m > 0$ to $C_i < 0$ at $Y = 0$, the whole expansion (141) up to the cubic order of Y is bounded from below and the free-energy minimum appears at a finite Y . Such jumps of the coefficients at $Y = 0$ clearly violate Ginzburg-Landau-Wilson scheme of phase transitions and indicate that the M I transition at $T = 0$ is not explained by the concept of the spontaneous symmetry breaking. The origin of the jumps is ascribed to the jump of the density of states from a nonzero value in metals to zero in insulators in two dimensions. It reflects the topological nature of the M I transition, which is caused by the disappearance (or emergence) of the Fermi surface without a change in the symmetry.

From the free-energy expansion in Eq. (141), we find that both continuous and first-order M I transitions occur at $T = 0$. The numerical estimates for the relevant parameter region of the extended Hubbard model show $B_i > 0$ and $B_i > B_m$, whereas $C_i < 0 < C_m$. When $B_m > 0$, the region $A < 0$ represents the metallic phase, while the insulating state is stabilized for $A > 0$. For $B_m > 0$, the M I transitions are always continuous. The quantum critical line with the continuous M I transition is determined by the condition $A = 0$. When B_m becomes zero, the quantum critical line terminates at the marginal quantum critical point (MQCP) [$A = 0, B_m = 0$] and the first-order transition line begins in the region $B_m < 0$. Our calculated coefficients A and B_m specify the locations of MQCP at $t^0 = 0.05571$ and $t^0 = 0.36455$ for the extended Hubbard model.

In Sec. 4, we have studied the M I transitions by solving the self-consistent equation numerically. The obtained phase diagram in t^0 - g plane at $T = 0$ contains two MQCPs. We have confirmed that the numerical results are consistent with the analytical results obtained in Sec. 3.

Our mean-field exponents at MQCP is essentially exact beyond the mean-field theory. Substituting these critical exponents to the Ginzburg criterion [9], we obtain the

upper critical dimensions d_c as

$$d_c = \frac{+2}{z} \quad z = 2:$$

Since the two-dimensional system is at the upper critical dimension, the mean-field critical exponents of MQCP should be exact except for possible logarithmic corrections.

Using the free-energy expansion in Eq. (141), we obtain the critical exponents of MQCP as $\beta = 1$, $\gamma = 1$, $\nu = 1$, $\eta = 2$, $\nu = 1/2$, $\nu = 0$ and the dynamical exponent $z = 4$ in the metallic side of the transition. These critical exponents show that MQCP belongs to an unconventional universality class different from those obtained from phase transitions caused by the spontaneous symmetry breaking.

The discontinuities of the coefficients B and C exist, in the strict sense, only at $T = 0$. At nonzero temperatures, the jump is immediately smeared out, which makes a crossover to a different universality. We find that the first-order M I transition boundary extends to nonzero temperatures and terminates at the critical point. Around the finite-temperature critical line, the free energy follows the GLW scheme. The criticality is perfectly categorized by the Ising universality. This means that the universality class of the finite-temperature transition may be characterized as a symmetry breaking transition in contrast to $T = 0$ transitions.

The peculiarity of the universality at MQCP is ascribed to the fact that MQCP appears as the marginal point between the conventional GLW transition at nonzero temperature with emergence of the spontaneous symmetry breaking, and the topological transition at $T = 0$, each of which are described by already known physics, while its connecting point is not. This unconventional universality class of MQCP is consistent with recent experimental results of $(\text{ET})_2\text{CuN}(\text{CN})_2\text{Cl}$. Although we have focused on the band-width control M I transitions, these critical exponents are the same as those of the filling-control M I transitions.

We have clarified how the crossover between Ising and MQCP universalities appears. It has been shown that even the finite-temperature critical point may show MQCP region when the parameter is tuned away from the narrow Ising region. This explains the experimental observation on the ET compound.

In this paper, we have considered only M I transitions in the ordered phase. We assume that a preexisting gap exists in the metallic phase because of the symmetry breaking. However, beyond the mean-field theory, even without the symmetry breaking, preexisting gap opens in the metallic phase as in the case of Mott insulator at low dimensions. Therefore, the consequence of the present mean-field treatment may survive without a strict order, where ϕ may be replaced with the correlation induced gap without long-range order. This is indeed corroborated by various numerical studies performed beyond the mean-field approximations, which consistently sup-

port the hyperscaling with $\nu = 2$ and $z = 4$.

The present results show that the MI transition is governed by the topological change of the Fermi surface, with shrinkage (or emergence) at selected momentum points. This is different from other types of mean-field theories such as the dynamical mean-field approximations, where the MI transition is governed instead by the vanishing renormalization factor Z . On the verge of the MI transition in the metallic side, it possibly means that the Fermi surface is reduced to small pockets which violates the Luttinger sum rule. If the system undergoes a Lifshitz transition from a large to small Fermi surface in the metallic phase, this violation is allowed in the side of small pockets. The improvement of the dynamical mean-field theory to include the momentum dependence indeed suggests the existence of such a Lifshitz transition as we discussed in Sec. I. The existence of the small Fermi surface without folding of the Brillouin zone in the absence of the translational symmetry breaking is a fundamental issue and should be more thoroughly studied in the future.

The present study has revealed a mechanism of generating quantum critical point of the metal-insulator transition, which has been unexplored in the literature. The marginal quantum critical point emerges because of the generation of the gap determined in cooperation with the kinetic energy gain of metallic carriers. Its combined and nonlinear effect yields pinning of the quasiparticle energy in contrast to the rigid band picture. This may be expressed by attractive effective interaction of carriers. It generates an unconventional universality.

A remarkable finding is that MQCP is governed by the coexistence of quantum fluctuations and the divergence of the density fluctuations at small wave numbers. Such density fluctuations may cause various further and deeper effects near MQCP. Its thorough understanding is an intriguing issue left for future studies. Among all, revealing momentum and frequency resolved density fluctuations is an extremely important challenging issue of experimental studies, which must reveal an anomalous and critical enhancement near MQCP as well as near the finite-temperature critical point if accurate measurements are made. Thorough studies of superconducting mechanism arising from MQCP [37] are also extremely important issue to be explored.

Acknowledgments

The authors are indebted to Youhei Yamaji for extensive discussions. The authors thank Hiroshi Fukuyama, Kazushi Kanoda and Fumitaka Kagawa for illuminating discussions on their experimental results. One of the authors (T.M.) thanks Shinji Watanabe for stimulating discussions. This work is supported by Grant-in-Aids for Scientific Research on Priority Areas under the grant numbers 17071003 and 16076212 from MEXT, Japan. A part of our computation in this work has been done using

the facilities of the Supercomputer Center, Institute for Solid State Physics, University of Tokyo.

APPENDIX A

In this appendix we show details of the numerical calculations. In the standard procedure of solving Eqs. (46) and (47), input parameters are effective interaction g and particle density n . In this procedure, chemical potential and the order parameter m are determined by solving Eqs. (46) and (47) self-consistently. This procedure costs much computation time, and is not efficient in determining g and m precisely.

Instead, we use a different procedure. Namely, we take g and n as input parameters, while output parameters are g and m . By following this procedure, first, in Eq. (47) for fixed k_y , we can determine the chemical potential μ to satisfy the condition $n = 1$ independent of Eq. (46). Then, using this μ , we perform the integration of the right hand side of Eq. (46) and obtain g . Finally, we obtain the order parameter $m = -g$. Since this procedure does not require the self-consistent calculations, it is possible to calculate Eqs. (46) and (47) rapidly and precisely.

Hereafter, we explain the details of integration of Eqs. (46) and (47). To calculate the k -space integration in Eq. (47), first we fix k_y and obtain the particle density integrated over k_x , namely $n(k_y)$. It is easy to solve the equation

$$2(k_x; k_y) \frac{g}{1(k_x; k_y)^2 + 2} = 0 \quad (\text{A1})$$

with respect to $\cos k_x$ for fixed k_y analytically since the equation is quadratic with respect to $\cos k_x$. Using the roots of the Eq. (A1), we obtain $n(k_y)$ exactly. To simplify the explanation, we only consider the case that the two real roots exist for upper band and their absolute values are less than 1. In this case, analytically we can obtain the location of the point where E_+ and E_- cross, namely k_x and $-k_x$ [see Fig. 19]. From this, for the upper [lower] band, the particle density for fixed k_y is given by $n(k_y)_+ = 2k_x = 2[n(k_y) = 2(k_y) = 2]$, where (k_y) is the edge of Brillouin zone. The particle density for the fixed k_y is given as $n(k_y) = n(k_y)_+ + n(k_y)_-$. In other cases, in a similar way, we can obtain $n(k_y)$ analytically. By integrating $n(k_y)$ over k_y , we obtain the whole particle density n . Along the k_y direction, we use Newton-Cotes formula and take the number of points in the k_y direction up to 400000.

Next, we explain the way of integrating over k in the right hand side of Eq. (46). We fix k_y and perform the k_x integration first. Along the k_x direction, we use double exponential (DE) formula, which is suitable for the integration of the analytic function in the integration period. It is known that DE formula is one of the optimized methods to integrate the analytic function with the highest accuracy using the smallest number of points. In the

above case, integration periods I_1 and I_2 are given as $I_1 = [-\Lambda; -k_r]$ and $I_2 = [k_r; \Lambda]$ (see Fig. 19). DE formula is useful in these periods, since the right hand side of Eq. (46) is analytical. We take the number of points in these periods up to 1000. Then we perform the integration over k_y using the Newton-Cotes formula, and obtain the effective interaction g . We take the number of points in the k_y -direction up to 400000 for the integration.

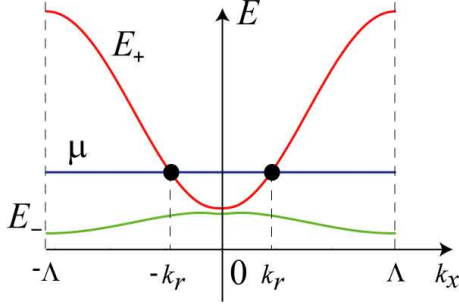


FIG. 19: (color online) Schematic band structure for fixed k_y . Circles represent the crossing points of the upper band and the chemical potential, which occur at k_r .

APPENDIX B

In this appendix we derive Eqs. (64), (65) and (66). First, we obtain the density of states (DOS) at the bottom (top) of the upper (lower) band, respectively.

The location of the bottom of the upper band is given by $(-\pi; 0)$ and $(0; \pi)$. Near $(-\pi; 0)$, using Eq. (44), E_+ is expanded with respect to $q_x = k_x$ and $q_y = k_y$ as

$$E_+ = \frac{4t^0 \cos q_x \cos q_y}{q} + \frac{4t^2 (\cos q_x - \cos q_y)^2 + t^2}{4} \quad (B1)$$

$$4t^0 + 2t^0 q^2; \quad (B2)$$

where we define $q = \sqrt{q_x^2 + q_y^2}$. From this, we obtain

$$\frac{dE_+}{dq} = 4q t^0. \quad (B3)$$

The DOS of the upper band near $(-\pi; 0)$ is given by

$$D_+ = \frac{1}{4 t^0}. \quad (B4)$$

Near the MI transition, the Fermi wave number q_f is determined by the condition

$$E_+ = 4t^0 + 2t^0 q_f^2 = 0; \quad (B5)$$

where μ is the chemical potential. From Eqs. (B2) and (B5), we obtain

$$q_f = \sqrt{\frac{2 t_c}{t^0}}; \quad (B6)$$

where $t_c = 2t^0$. Using this, the electron density of the upper band, namely electron density X_+ including spin degeneracy is given by

$$X_+ = \frac{q_f^2}{2} = \frac{1}{2} \frac{2 t_c}{t^0} = \frac{t_c}{t^0}; \quad (B7)$$

The location of the top of the lower band is given by $(\pi; \pi)$ and its equivalent points. Near $(\pi; \pi)$, using Eq. (44), E_- is expanded with respect to $q_x = \pi - k_x$ and $q_y = \pi - k_y$, which leads to

$$E_- = -2t^0 \left(t^0 \sin \frac{t^2 (1 + \sin 2)}{t^0} \right); \quad (B8)$$

where we define $q = \sqrt{q_x^2 + q_y^2}$. Then we obtain

$$\frac{dE_-}{dq} = 4q \left(t^0 \left(\frac{t^2}{t^0} \right) \sin 2 \right); \quad (B9)$$

From Eq. (B9), the DOS of the lower band near $(\pi; \pi)$ is given by

$$D_- = \frac{8}{(2 t^0)^2} \frac{1}{4 \left(\frac{t^2}{t^0} \right) \sin 2} = \frac{1}{2 t^0 \frac{t^2}{t^0} \sin 2}; \quad (B10)$$

Near the MI transition, the Fermi wave number q_f is determined by the condition

$$E_- = -2t^0 \left(t^0 \sin \frac{t^2 (1 + \sin 2)}{t^0} \right) = 0; \quad (B11)$$

where μ is the chemical potential. From Eqs. (B8) and (B11), we obtain

$$q_f = \sqrt{\frac{t^0 \left(\frac{t^2}{t^0} \right)}{t^2 \left(\frac{t^2}{t^0} \right) \sin 2}}; \quad (B12)$$

Using this, the hole density of the lower band, namely the hole density X_- is given by

$$X_- = \frac{4}{4 t^0} \frac{1}{4 \left(\frac{t^2}{t^0} \right) \sin 2} = \frac{1}{2 t^0 \frac{t^2}{t^0} \sin 2}; \quad (B13)$$

At half filling, X_+ should be equal to X_- . From this condition, recalling Eq. (63) and using Eqs. (B7) and (B13), we obtain ~ as

$$\sim = \frac{2t^0}{2t^0 + \frac{t^2}{t^0}}; \quad (B14)$$

- [1] M. Imada, A. Fujimori, and Y. Tokura, *Rev. Mod. Phys.* **70**, 1039 (1998).
- [2] M. Imada, *J. Phys. Soc. Jpn.* **63**, 4294 (1994).
- [3] M. Imada, *J. Phys. Soc. Jpn.* **64**, 2954 (1995).
- [4] L. S. Ornstein and F. Zernike, *Proc. Acad. Sci. (Amsterdam)* **17**, 793 (1914).
- [5] A. Einstein, *Ann. Phys.* **33**, 1276 (1910).
- [6] M. Smoluchowski, *Ann. Phys.* **25**, 205 (1908).
- [7] L. D. Landau, E. M. Lifshitz and E. M. Pitaevskii, *Statistical Physics* (Butterworth-Heinemann, New York, 1999).
- [8] Wilson, K. G. The renormalization group and critical phenomena *Rev. Mod. Phys.* **55**, 583 (1983).
- [9] For a textbook, see N. G. Goldenfeld : *Lectures on Phase Transitions and Renormalization Group* (Addison-Wesley, 1992).
- [10] R. J. Elliott, *J. Phys. C* **4**, 2359 (1971).
- [11] T. Moriya, *Spin Fluctuations in Itinerant Electron Magnetism* (Springer-Verlag, Berlin, 1985).
- [12] J. A. Hertz, *Phys. Rev. B* **14**, 1165 (1976).
- [13] A. J. Millis, *Phys. Rev. B* **48**, 7183 (1993).
- [14] A. J. Millis, A. J. Schofeld, G. G. Lonzarich, and S. A. Grigera, *Phys. Rev. Lett.* **88**, 217204 (2002).
- [15] X.-G. Wen, *Ann. Phys.* **316**, 1 (2005).
- [16] J. Hubbard, *Proc. Roy. Soc. London* **276**, 238 (1963); *ibid* **227**, 237 (1964); *ibid* **281**, 401 (1964).
- [17] W. F. Brinkman and T. M. Rice, *Phys. Rev. B* **2**, 4302 (1970).
- [18] A. Georges, G. Kotliar, W. Krauth, and M. J. Rozenberg, *Rev. Mod. Phys.* **68**, 13 (1996).
- [19] S. Onoda and M. Imada, *Phys. Rev. B* **67**, 161102(R) (2003).
- [20] K. Hanasakia and M. Imada, *J. Phys. Soc. Jpn.* **75**, 084702 (2006).
- [21] S. Onoda and M. Imada, *J. Phys. Chem. Solids* **63**, 2225 (2001).
- [22] M. Imada and S. Onoda, *J. Phys. Chem. Solids* **62**, 47 (2002).
- [23] T. Yoshida, X. J. Zhou, T. Sasagawa, W. L. Yang, P. V. Bogdanov, A. Lanzara, Z. Hussain, T. Mizokawa, A. Fujimori, H. Eisaki, Z.-X. Shen, T. Kakeshita, and S. Uchida, *Phys. Rev. Lett.* **91**, 027001 (2003).
- [24] N. P. Armitage, F. Ronning, D. H. Lu, C. Kim, A. Damascelli, K. M. Shen, D. L. Feng, H. Eisaki, Z.-X. Shen, P. K. Mang, N. Kaneko, M. Greven, Y. O. Nozue, Y. Taguchi, and Y. Tokura, *Phys. Rev. Lett.* **88**, 257001 (2002).
- [25] C. Berthod, T. Giamarchi, S. Biermann, and A. Georges, cond-mat/0602304.
- [26] Th. A. Maier, Th. Pruschke and M. Jarrell, *Phys. Rev. B* **66**, 075102 (2002).
- [27] M. Cicivelli, M. Capone, S. S. Kancharla, O. Parcollet, and G. Kotliar, *Phys. Rev. Lett.* **95**, 106402 (2005).
- [28] For instance, in Refs.[1, 3], the control parameter was taken as c , while here, it is taken as g , which turns out to be scaled by $(c)^{1/2}$ for the marginal quantum critical point of the filling-control transition in two dimensions. This makes a trivial factor two necessary for the present $\nu = 1/2$ in comparison with $\nu = 1/4$ in Refs.[1, 3], although z is common only 4. Along the quantum critical line, this factor two is not necessary, because c is scaled linearly with g . The scaling between g and c will be clarified in Sec.2. The exponent $\nu = 2/(d+z)$ in the present definition is $\nu = 2/(d+z)=2$ while it is $\nu = 2/(d+z)=4$ in Refs.[1, 3]. In any case, these transformations do not make any difference in scalings of real physical quantities.
- [29] N. Furukawa and M. Imada, *J. Phys. Soc. Jpn.* **60**, 3604 (1991).
- [30] N. Furukawa and M. Imada, *J. Phys. Soc. Jpn.* **61**, 3331 (1992).
- [31] N. Furukawa and M. Imada, *J. Phys. Soc. Jpn.* **62**, 2557 (1993).
- [32] M. Kohno, *J. Phys. Soc. Jpn.* **55**, 1435 (1997).
- [33] H. Nakano and M. Imada, *J. Phys. Soc. Jpn.* **68**, 1458 (1999).
- [34] H. Tsunetsugu and M. Imada, *J. Phys. Soc. Jpn.* **67**, 1864 (1998).
- [35] S. Watanabe and M. Imada, *J. Phys. Soc. Jpn.* **73**, 1251 (2004).
- [36] M. Imada, *J. Phys. Soc. Jpn.* **73**, 1851 (2004).
- [37] M. Imada, *J. Phys. Soc. Jpn.* **74**, 859 (2005).
- [38] M. Imada, *Phys. Rev. B* **72**, 075113 (2005).
- [39] N. Harima, A. Fujimori, T. Sugaya and I. Terasaki, *Phys. Rev. B* **67**, 172501 (2003).
- [40] H. Yagi, T. Yoshida, A. Fujimori, Y. Kohsaka, M. Misawa, T. Sasagawa, H. Takagi, M. Azuma and M. Takano, *Phys. Rev. B* **73**, 172503 (2006).
- [41] A. Casey, H. Patel, J. Nyeki, B. P. Cowan, and J. Saunders, *Phys. Rev. Lett.* **90**, 115301 (2003).
- [42] G. Kotliar, E. Lange, and M. J. Rozenberg, *Phys. Rev. Lett.* **84**, 5180 (2000).
- [43] C. Castellani, C. Di Castro, D. Feinberg, and J. Ranninger, *Phys. Rev. Lett.* **43**, 1957 (1979).
- [44] P. Linette, A. Georges, D. Jerome, P. Wzietek, P. Metcalf, and J. M. Honig, *Science* **302**, 89 (2003).
- [45] F. Kagawa, T. Itou, K. Miyagawa, and K. Kanoda, *Phys. Rev. B* **69**, 064511 (2004).
- [46] F. Kagawa, K. Miyagawa, and K. Kanoda, *Nature* **436**, 534 (2005).
- [47] H. Kondo and T. Moriya, *J. Phys. Soc. Jpn.* **65**, 2559 (1996).
- [48] W. Hofstadter and W. Vollhardt, *Ann. Phys.* **7**, 48 (1998).
- [49] T. Misawa, Y. Yamaji, and M. Imada, *J. Phys. Soc. Jpn.* **75**, 083705 (2006).
- [50] Detailed derivation will be given elsewhere.
- [51] The critical exponent ν also characterizes the singularity of the order parameter with respect to the control parameter. Namely, we can define ν as X/a , where X is the order parameter and a is a control parameter. In this definition, ν is well defined even in the case of the continuous MIT transitions. In this case, since the control parameter is equivalent to the external field, ν is equal to $\nu = 1$. In Ref. [8], this definition is chosen.
- [52] T. Moriya, H. Morita, and S. Tanaka, *Bull. Chem. Soc. Jpn.* **72**, 179 (1999).
- [53] K. Miyagawa, K. Kanoda, and A. Kawamoto, *Chem. Rev.* **104**, 5635 (2004).
- [54] Y. Matsumoto, D. Tsuji, S. Murakawa, H. Akisato, H. Kambara and H. Fukuyama, *J. Low Temp. Phys.* **138**, 271 (2005).